

# Measurement-based quantum computation in finite one-dimensional systems: string order implies computational power

Robert Raussendorf, Wang Yang and Arnab Adhikary

*Department of Physics & Astronomy, University of British Columbia, Vancouver, Canada,  
Stewart Blusson Quantum Matter Institute, University of British Columbia, Vancouver, Canada*

November 15, 2022

## Abstract

We present a new framework for assessing the power of measurement-based quantum computation (MBQC) on short-range entangled symmetric resource states, in spatial dimension one. It requires fewer assumptions than previously known. The formalism can handle finitely extended systems (as opposed to the thermodynamic limit), and does not require translation-invariance. Further, we strengthen the connection between MBQC computational power and string order. Namely, we establish that whenever a suitable set of string order parameters is non-zero, a corresponding set of unitary gates can be realized with fidelity arbitrarily close to unity.

## 1 Introduction

Resource states for measurement-based quantum computation (MBQC) [1] are known to be rare in Hilbert space [2]. But symmetry adds a twist to this picture. When symmetries are present, in the thermodynamic limit, short-range entangled quantum states group into so-called *computational phases of quantum matter* [3–7]. From a condensed matter perspective, these phases are symmetry protected topologically (SPT) ordered [8–12]. From the perspective of quantum computation, these phases are warehouses full of MBQC resource states. Any quantum state in a given SPT phase can be used to realize quantum computations, and, moreover, the *same* quantum computations. The power of MBQC across SPT phases is uniform [14–21].

The phenomenology of MBQC becomes richer with increasing spatial dimension of the resource states: one dimension (1D) is mostly a test bed for computational methods, 2D reaches quantum computational universality [1, 22, 23], and 3D combines universality with fault-tolerance [13]. This increase of computational power with dimension is matched in computational phases. The first such phases were identified in 1D [14–17], capable of processing a bounded number of logical qubits. In 2D, examples of universal computational phases are known [18–21]. In 3D, the fault-tolerance capability of cluster states has been related to SPT order with 1-form symmetry [24]. As the phenomenology flourishes with increasing dimension, our understanding diminishes: In spatial dimension one, a classification scheme for computational phases exists [15–17]; and furthermore a gauge principle underlying MBQC has been identified [25]. In higher dimensions we have several examples for computational phases, but no classification.

For the reasons just outlined, most current research on the subject of computational phases of quantum matter focuses on higher dimensions. Nonetheless, in the present paper we return to the one-dimensional case—with the intention of later applying what we learn to 2D and 3D.

We investigate resource states for measurement based quantum computation that are (i) short-range entangled in dimension one, (ii) of finite size, and (iii) invariant under the action of a symmetry group  $(\mathbb{Z}_2)^m$ . The works to date have mostly focused on computational phases of quantum matter, requiring the thermodynamic limit. In contrast, here we specifically ask: *What happens to computational power if we transition from infinite to finite systems?* This is an important question: Quantum computing is about efficiency, hence resource counting. The finite size of an MBQC resource state is thus an essential property.

As it turns out, the above is also a conceptually fruitful question, as it prompts us to adopt a novel perspective. Namely, in the discussion of computational phases of matter to date [7, 14–21], the resource state is the primary object, the object to classify. The measurement procedure that extracts computational power is almost an afterthought. Here, we turn this picture on its head. Since phases—symmetry-protected, computational, or otherwise—are not defined in finite systems, they can no longer be the basis for classification. This is a priori a detriment, for the classification of 1D SPT phases in terms of group cohomology [8–12] is very beautiful, and also the basis for the “SPT-to-MBQC meat grinder” [15, 16], which converts cohomological data into MBQC schemes. As we show in this paper, in the new situation of finite system size, the measurement procedure takes over as the primary object, the object suited to classification. Projective representations, and their cohomological classification, reappear in it. The resource states, in turn, become the accessory in the formalism. They have to be short-range entangled, symmetric, and possess string order matching the symmetry. That’s all there’s to say about them.

Our technical findings are two-fold: (I) We demonstrate that in one-dimensional finite systems, computational order is string order [26–28], and (II) We devise a more broadly applicable and flexible formalism for reasoning about symmetric, short-range entangled quantum states as resources for MBQC. The advantages of the new formalism are described in detail in Section 2.

We remark that the formalism developed in this paper is not based on matrix product states [30], as previous results [7, 14–21] on computational phases of quantum matter are. Rather, it has a quantum coding theoretic flavour.

The remainder of this paper is organized as follows. In Section 2 we describe the above-listed advances in greater detail. In Section 3 we define our setting, and introduce the four examples through which we will subsequently illustrate our result, namely the cluster chain, the Kitaev-Gamma chain, a spin chain relating to the output of a Clifford quantum cellular automaton (QCA), and the Ising chain with transverse magnetic field. In Section 4 we state and prove our main result, Theorem 1. It says that multi-particle quantum states can be used as resources for measurement based quantum computation if they (a) are invariant under a suitable group of symmetries, (b) are short-range entangled, and (c) have non-vanishing string order parameters of a form matching the symmetries. We apply the theorem to the examples introduced in the previous section. Section 5 is about block locality vs. site locality. Here we treat the cluster chain and the QCA chain in a refined fashion, leading to blocks of size one. In Section 6 we discuss the relation between string order parameters and the computational order parameters defined in [15]. In Section 7 we relate string order to quantum contextuality. Section 8 is the conclusion.

## 2 Advances of the new formalism

We now explain the advances made by the new formalism.

(1) *Computational order equals string order:* The relevance of string operators for the functioning of MBQC was first recognized in [3, 4]. In [4], quantum correlations describing the fidelity of gate simulations in MBQC were expressed in terms of string operators. In [3], it was shown for

ground states of the transverse field cluster model, the gate fidelity is bounded from below by a constant.

Here, we strengthen the above connection. Namely we show that whenever the string order parameters are *non-zero*, quantum gates can be realized in MBQC with fidelity arbitrarily close to unity. The higher the fidelity targeted, the larger the section of resource state consumed in the implementation of the gate.

In prior analysis of MBQC on resources states taken from SPT phases [15,16], in the framework of MPS, a computational order parameter  $\nu$  was identified that governs the operational overheads of MBQC. It was shown in [15] how to extract this order parameter from the MPS tensor representing the resource quantum state, but no physical interpretation for it had been found. We now realize that the computational order parameter  $\nu$  and the string order parameter are the same.

(2) *Block size*: In the discussion of SPT and MBQC by the MPS formalism, neighbouring spins are grouped into blocks [7, 14–20], such that the action of the symmetry group on each block is faithful. The block thereby becomes the natural local unit for the formalism.

In all cases so far considered, the blocks comprise more than a single spin, and this leads to a mismatch from the perspective of MBQC phenomenology. Namely, in standard MBQC, the local unit is a single spin. The measurements driving an MBQC are supposed to be site-local, not just block local. There is thus a gap between the MPS formalism and the phenomenology of interest. In the prior discussions of 1D, the block size is only 2; a gap that was deemed minor. In 2D, however, the block size increases with system size, leading to a very weak result about computational phases of quantum matter if left unaddressed. Therefore, in [18–20], supplemental arguments have been put on top of the basic formalism to reach block size one.

The present formalism doesn't require faithfulness of the representations involved, and can therefore handle blocks of any size down to size one. The physically motivated single-site locality of MBQC can be matched by the present formalism in its very algebraic structure, without the need for add-on arguments.

(3) *Translation invariance*: The prior formalism [7,14–20] requires translation invariance whereas the present formalism doesn't. Translation invariance is tied to the thermodynamic limit: no finite chain is translation-invariant. Therefore, getting rid of the constraint of translation invariance is a precondition for discussing finite systems.

The present formalism achieves this, and in fact permits much greater flexibility than merely permitting the existence of boundaries. For example, the value of the string order parameter may vary with the location of its end point in any fashion.

### 3 The setting

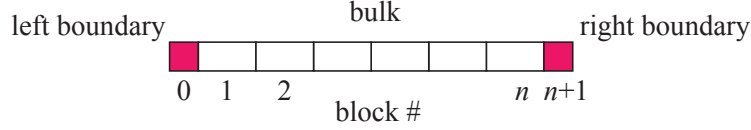
In this section we define our setting of short-range entangled symmetric states, and introduce the examples that we will subsequently use to illustrate our main theorem.

#### 3.1 Symmetric short-range entangled states

As our fundamental notion of “short-range entangled”, we use that of short-range, bounded depth quantum circuits applied to a product state. Two quantum states are considered equivalent under a given symmetry  $G$  if they can be related by a  $G$ -symmetric such circuit. This is an operationally well-motivated notion in the context of quantum computation.

We consider quantum states  $|\Phi\rangle$  on open chains of spin 1/2 particles. The support of the states  $|\Phi\rangle$  is grouped into  $n$  blocks in the bulk, plus a block 0 on the left boundary and a block  $n + 1$  on

the right boundary. Graphically,



The states  $|\Phi\rangle$  are short-range entangled and  $G$ -symmetric.

**Symmetry.** The symmetry group  $G$  discussed in this paper is of the form  $G = (\mathbb{Z}_2)^m$ . It acts via a linear representation  $U$  on  $|\Phi\rangle$ ,

$$U(g)|\Phi\rangle = (-1)^{\chi(g)}|\Phi\rangle, \quad \chi(g) \in \mathbb{Z}_2, \quad \forall g \in G. \quad (1)$$

**Entanglement structure.** The resource states  $|\Phi\rangle$  we consider are all of the form

$$|\Phi\rangle = W_\Phi(|+\rangle|+\rangle \dots |+\rangle). \quad (2)$$

Therein,  $W_\Phi$  is a bounded-depth circuit composed of bounded-range gates. We quantify the short-range entangling nature of  $W_\Phi$  as follows. We define two subsets of particle block labels on the line,

$$\{\leq k\} := \{0, 1, 2, \dots, k\}, \quad \{> k\} := \{k+1, k+2, \dots, n+1\}.$$

The short-range nature of  $W_\Phi$  is specified by an entanglement range  $\Delta$ . Denoting by  $\text{supp}(A)$  the support of a linear operator  $A$  on the line segment  $\{1, \dots, n\}$ , we make the following definition.

**Definition 1** *The entanglement range  $\Delta$  of a quantum circuit  $W_\Phi$  acting on the spin chain  $\{0, \dots, n+1\}$  is the smallest integer  $\Delta \geq 0$  such that, for all  $k = 0, \dots, n+1$ , it holds that*

$$\begin{aligned} \text{supp}(W_\Phi^\dagger A W_\Phi) &\subset \{\leq (k + \Delta)\}, \quad \forall A | \text{supp}(A) \subset \{\leq k\}, \\ \text{supp}(W_\Phi^\dagger A W_\Phi) &\subset \{> (k - \Delta)\}, \quad \forall A | \text{supp}(A) \subset \{> k\}. \end{aligned} \quad (3)$$

The short-range entanglement in resource states  $|\Phi\rangle$  enters MBQC through the following lemma.

**Lemma 1** *Consider a short-range entangled state  $|\Phi\rangle = W_\Phi|+\rangle|+\rangle \dots |+\rangle$ , where the circuit  $W_\Phi$  has an entanglement range  $\Delta$ . Be  $A$  and  $B$  two linear operators, with their support contained in  $\{\leq (k - \Delta)\}$  and  $\{> (k + \Delta)\}$ , respectively, for any  $k = \Delta, \dots, n+1 - \Delta$ . Then it holds that*

$$\langle \Phi | AB | \Phi \rangle = \langle \Phi | A | \Phi \rangle \langle \Phi | B | \Phi \rangle. \quad (4)$$

*Proof of Lemma 1.* We define  $\mathcal{L} := \{\leq k\}$ ,  $\mathcal{R} := \{> k\}$ , and write the product state to which the short-range circuit  $W_\Phi$  is applied as  $|+\rangle_{\mathcal{LR}} := |+\rangle_{\mathcal{L}} \otimes |+\rangle_{\mathcal{R}}$ , with  $|+\rangle_{\mathcal{L}} = |+\rangle_0 \otimes \dots \otimes |+\rangle_k$  and  $|+\rangle_{\mathcal{R}} = |+\rangle_{k+1} \otimes \dots \otimes |+\rangle_{n+1}$ . Therein,  $|+\rangle_i$  is the eigenstate with eigenvalue 1 of the Pauli observables  $X_j$ , for all sites  $j$  in the block  $i$ . Only locality between the left half  $\mathcal{L}$  and the right half  $\mathcal{R}$  of the chain, split between blocks  $k$  and  $k+1$ , matters.

We observe that, with the assumptions of the Lemma and Eq. (3) it holds that  $\text{supp}(W_\Phi^\dagger A W_\Phi) \subseteq \mathcal{L}$  and  $\text{supp}(W_\Phi^\dagger B W_\Phi) \subseteq \mathcal{R}$ ; hence

$$W_\Phi^\dagger A W_\Phi = W_\Phi^\dagger A W_\Phi|_{\mathcal{L}} \otimes I_{\mathcal{R}}, \quad W_\Phi^\dagger B W_\Phi = I_{\mathcal{L}} \otimes W_\Phi^\dagger B W_\Phi|_{\mathcal{R}}. \quad (5)$$

We then have

$$\begin{aligned}
\langle \Phi | AB | \Phi \rangle &= \mathcal{L} \langle + | \otimes_{\mathcal{R}} \langle + | W_{\Phi}^{\dagger} A B W_{\Phi} | + \rangle_{\mathcal{L}} \otimes | + \rangle_{\mathcal{R}} \\
&= \mathcal{L} \langle + | \otimes_{\mathcal{R}} \langle + | \left( W_{\Phi}^{\dagger} A W_{\Phi} \right) \left( W_{\Phi}^{\dagger} B W_{\Phi} \right) | + \rangle_{\mathcal{L}} \otimes | + \rangle_{\mathcal{R}} \\
&= \mathcal{L} \langle + | W_{\Phi}^{\dagger} A W_{\Phi} \Big|_{\mathcal{L}} | + \rangle_{\mathcal{L}} \mathcal{R} \langle + | W_{\Phi}^{\dagger} B W_{\Phi} \Big|_{\mathcal{R}} | + \rangle_{\mathcal{R}} \\
&= \mathcal{L} \mathcal{R} \langle + | W_{\Phi}^{\dagger} A W_{\Phi} | + \rangle_{\mathcal{L}} \mathcal{R} \mathcal{L} \langle + | W_{\Phi}^{\dagger} B W_{\Phi} | + \rangle_{\mathcal{R}} \mathcal{L} \mathcal{R} \\
&= \langle \Phi | A | \Phi \rangle \langle \Phi | B | \Phi \rangle.
\end{aligned}$$

Therein, in the third line we have used Eq. (5).  $\square$

*Remark:* The prior MPS formalism for reasoning about computational phases of quantum matter has at its base the MPS tensor identity for  $G$ -symmetric states

$$\begin{array}{c} u(g) \\ | \\ \boxed{A} \end{array} = V(g) \begin{array}{c} | \\ \boxed{A} \\ | \end{array} V(g)^{\dagger}, \quad (6)$$

where  $u(G)$  is a linear representation the symmetry group  $G$ , and  $V(G)$  a projective representation, characterized by a corresponding cohomology class [8–10,12]. The states Eq. (2) of the present setting are short-range entangled, with their MPS representation having a fixed bond dimension, independent of the size of the chain. Thus, by Corollary 2 of [29], Eq. (6) holds, and the formalism developed in Refs. [15,16] can be applied. However, it comes with the added assumption of translation-invariance, and block-size larger than one.

### 3.2 The role of Hamiltonians in our setting and examples

A comment about the role of Hamiltonians and their ground states in measurement based quantum computation is now in order. From a fundamental point of view, MBQC has nothing to do with Hamiltonians at all; it is only about states and measurements. However, Hamiltonians do find a role to play, in the following way. It has been observed [2] that, when sampled uniformly from Hilbert space, computationally useful resource states are extremely rare. This prompted the question: If so, then what about quantum states that naturally occur? A common notion of ‘naturally occurring’ is ground states of simple Hamiltonians. In this direction it has been established, for example, that AKLT states in dimension two are universal [22,23]. Moreover, entire SPT phases of matter can have computational power [14–17] and even be universal [18–20].

The relation of the above works on computational phases of quantum matter to the present paper is that, in 1D, ground states of gapped local Hamiltonians approximately satisfy condition Eq. (3), with an approximation error that exponentially decreases with the range parameter  $\Delta$ .

However, the focus of this paper is on quantum states that satisfy condition Eq. (3) *exactly*. It is those states that we derive our main results for—Theorem 1 and Corollary 1 in Section 4.3. We have an operational motivation for considering these states, independent of computational phases of quantum matter. Namely, they can be efficiently created by bounded-depth circuits with short-range gates. There is no reference to Hamiltonians and their ground states in this formulation. Nonetheless, based on the above correspondence, we will use ground states as physically intuitive examples approximately realizing our conditions.

### 3.3 Examples

Here we introduce four examples for SPT phases, and transitions between them. We will subsequently use them to illustrate the corresponding MBQC quantum computational power. The

examples are (i) the cluster chain, (ii) the Kitaev-Gamma chain, (iii) a spin chain related to quantum cellular automata, and (iv) the Ising chain.

All four examples are based on ground states of 1D local Hamiltonians. Ground states of gapped local Hamiltonians have exponential decay of correlations [31]. Thus they only approximately realize the above notion of ‘short-range entangled’, with an accuracy exponentially increasing with the length scale  $\Delta$ . We use these examples in spite of the approximation, to make the connection to known 1D physics.

### 3.3.1 The cluster chain

The cluster state is the “standard” resource in measurement based quantum computation. Cluster states in spatial dimension two are computationally universal [1]. In the simpler one-dimensional case that we discuss here, a single logical qubit can be simulated. The 1D cluster state lies inside a symmetry protected topological (SPT) phase with symmetry group  $\mathbb{Z}_2 \times \mathbb{Z}_2$ . It was demonstrated in [7] that the ability to perform measurement based quantum computational wire extends from the cluster state to the entire SPT phase surrounding it. Subsequently, the same was shown for computational capability; it too is uniform across the  $\mathbb{Z}_2 \times \mathbb{Z}_2$  cluster phase [15, 16].

We now define the 1D cluster state and its surrounding phase. We consider a chain of  $N$  spins  $1/2$ . W.l.o.g. we choose  $N$  odd. The cluster state  $|\mathcal{C}\rangle$  is a stabilizer state, constrained by the eigenvalue equations

$$Z_{i-1}X_iZ_{i+1}|\mathcal{C}\rangle = |\mathcal{C}\rangle, \quad i = 2, \dots, N-1$$

in the bulk, and

$$X_1Z_2|\mathcal{C}\rangle = Z_{N-1}X_N|\mathcal{C}\rangle = |\mathcal{C}\rangle$$

at the boundary. The above stabilizer constraints specify the cluster state uniquely, up to a global phase.

**Symmetry.** The stabilizer is an Abelian group, with a subgroup

$$G = \mathbb{Z}_2 \times \mathbb{Z}_2 \cong \langle ZXIXIXIX\dots IXZ, XIXIXIXI\dots IX \rangle. \quad (7)$$

$G$  is the symmetry group of interest. The cluster phase is the phase of  $G$ -symmetric states that contains the cluster state.

To assess computational power, we consider the order parameters

$$\begin{aligned} \sigma_e &= \langle I\dots IZXIXI\dots IX \rangle, \\ \sigma_o &= \langle I\dots IZXIXI\dots IXZ \rangle, \\ \sigma_{o+e} &= \langle I\dots IZYXX\dots XXY \rangle. \end{aligned} \quad (8)$$

For  $\sigma_e$  and  $\sigma_{o+e}$ , the left-most Pauli operator  $Z$  is located on an even-numbered qubit, and for  $\sigma_o$  on an odd-numbered qubit.

We show later that the expectation values  $\sigma_o$ ,  $\sigma_e$  and  $\sigma_{o+e}$  are associated with logical rotations generated by  $\sigma_z$ ,  $\sigma_x$  and  $\sigma_y$ , respectively. To implement such rotations, the expectation values of Eq. (8) must be non-zero.

For illustration, we consider a one-dimensional line in the phase diagram of  $\mathbb{Z}_2 \times \mathbb{Z}_2$ -symmetric states. Namely, we consider the ground states of the cluster Hamiltonian with magnetic field,

$$H(\alpha) = -\cos \alpha \left( X_1Z_2 + Z_{N-1}X_N + \sum_{i=2}^{N-1} Z_{i-1}X_iZ_{i+1} \right) - \sin \alpha \sum_{i=2}^{N-1} X_i, \quad (9)$$

parametrized by an interpolation parameter  $\alpha$ .

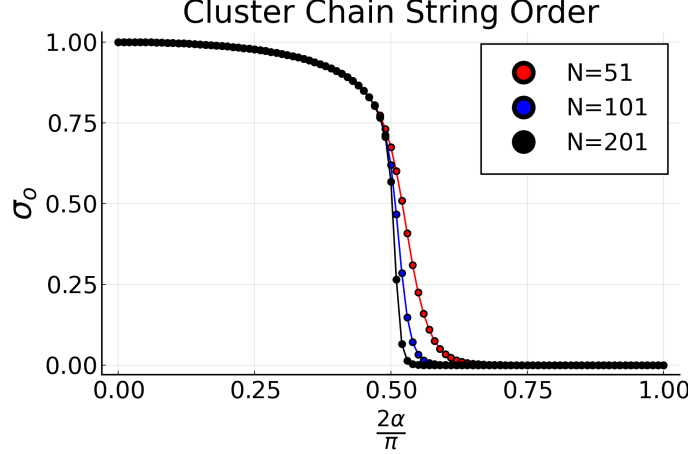


Figure 1: Order parameter  $\sigma_o$  as a function of the sweep parameter  $\alpha$  for the transverse field cluster Hamiltonian. The starting point of the string orders is deep in the bulk around  $N/4$ . The multiplicity of the curves is due to differing values of the chain length  $N$ . The plot for  $\sigma_e$  is indistinguishable to the naked eye from the above curves and is therefore omitted.

**Phase diagram.** When  $\alpha = 0$ , the ground state is a 1D cluster state. When  $\alpha = \pi/2$ , then the ground state is fourfold degenerate,  $|g(\pi/2)\rangle = |\pm\rangle_1|+\rangle_2\cdots|+\rangle_{N-1}|\pm\rangle_N$ . At  $\alpha = \pi/4$  occurs a change-over from cluster-like states to trivial (unentangled) states. This change-over is marked by the string order parameters  $\sigma$  changing from non-zero to zero. The larger the chain length  $N$ , the sharper the drop. In the thermodynamic limit, the change-over becomes a phase transition. See Fig. 1 for a plot of the order parameters as a function of  $\alpha$ .

### 3.3.2 The Kitaev-Gamma chain

One-dimensional Kitaev spin models [32–37] are 1D versions of the generalized Kitaev spin-1/2 models on the honeycomb lattice [38, 39] used to describe real Kitaev materials [40–44]. Besides providing useful information for the 2D Kitaev physics [37], 1D Kitaev models have intricate non-symmorphic symmetry group structures [33, 34, 36], and contain rich strongly correlated physics, including emergent conformal symmetries [33], nonlocal string order parameters [35] and exotic symmetry breaking phases [33–35], which make such 1D studies intriguing on their own.

**Model.** The model that we consider is the 1D spin-1/2 bond-alternating Kitaev-Gamma model [35, 36]. After applying a unitary transformation  $U_6$ , the system is called in the rotated frame and the Hamiltonian acquires the form [33]

$$H'_{K\Gamma} = \sum_{\gamma=\langle ij \rangle} g_\gamma [-K S_i^\gamma S_j^\gamma - \Gamma(S_i^\alpha S_j^\alpha + S_i^\beta S_j^\beta)], \quad (10)$$

in which:  $S_i^x = \frac{1}{2}X_i$ ,  $S_i^y = \frac{1}{2}Y_i$ ,  $S_i^z = \frac{1}{2}Z_i$  are the spin-1/2 operators on site  $i$ ;  $\gamma \in \{x, y, z\}$  is the spin direction associated with the bond connecting the nearest neighboring sites  $i$  and  $j$  as shown in Fig. 2;  $(\gamma, \alpha, \beta)$  (all belonging to  $\{x, y, z\}$ ) form a local right-handed coordinate system in spin space for sites  $i$  and  $j$  connected by the bond  $\gamma$ ;  $K$  and  $\Gamma$  are the Kitaev and Gamma interactions, respectively; and  $g_\gamma > 0$  ( $\gamma = x, y$ ) is the parameter for the bond strength on  $\gamma$ -

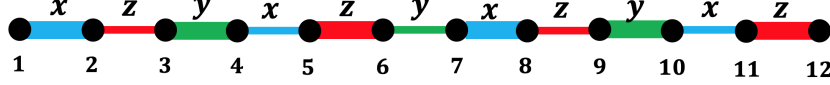


Figure 2: Bond pattern for the 1D bond-alternating Kitaev-Gamma model in the rotated frame. The thick and thin lines represent the alternating pattern of the bond strengths.

bond. The Hamiltonian  $H_{K\Gamma}$  before the  $U_6$  transformation and the definition of  $U_6$  are included in Appendix B.

**Symmetry.** The Hamiltonian  $H'_{K\Gamma}$  has an intricate symmetry group structure [36]. Namely,  $H'_{K\Gamma}$  is invariant under  $T$ ,  $U(R_{2a})T_{2a}$ ,  $U(R_M)M$ ,  $U(R(\hat{x}, \pi))$ ,  $U(R(\hat{y}, \pi))$ , and  $U(R(\hat{z}, \pi))$ , where  $T : S_i^\alpha \rightarrow -S_i^\alpha$  ( $\alpha = x, y, z$ ) is the time reversal operation;  $T_{ma} : S_i^\alpha \rightarrow S_{i+m}^\alpha$  is the translation operation by  $m \in \mathbb{Z}$  lattice sites;  $M : S_i^\alpha \rightarrow S_{7-i}^\alpha$  is the spatial inversion operation with the inversion center located at the middle point between sites 3 and 4;  $R(\hat{n}, \phi)$  is a global SU(2) spin rotation around  $\hat{n}$ -direction by an angle  $\phi$ ;  $R_{2a} = R(\frac{1}{\sqrt{3}}(1, 1, 1), \frac{2\pi}{3})$ ;  $R_M = R(\frac{1}{\sqrt{2}}(1, 0, -1), \pi)$ ; and  $U$  is the representation of the SU(2) group on the Hilbert space of the whole spin chain. Clearly, the symmetry group  $G_{K\Gamma}$  of  $H'_{K\Gamma}$  contains a  $\mathbb{Z}_2 \times \mathbb{Z}_2$  subgroup generated by  $\{U(R(\hat{z}, \pi)), U(R(\hat{x}, \pi))\}$ , where the explicit expression of  $U(R(\hat{\alpha}, \pi))$  ( $\alpha \in \{x, y, z\}$ ) is

$$U(R(\hat{\alpha}, \pi)) = \Pi_{i=1}^N 2S_i^\alpha \quad (11)$$

in which  $N \in 2\mathbb{Z}$  is the length of the chain. More generally, it has been proved in Ref. [36] that  $G_{K\Gamma}$  satisfies the following short exact sequence,

$$1 \rightarrow \langle T_{6a} \rangle \rightarrow G_{K\Gamma} \rightarrow O_h \rightarrow 1, \quad (12)$$

in which  $\langle T_{6a} \rangle$  denotes the group generated by  $T_{6a}$ , and  $O_h \cong S_4 \times \mathbb{Z}_2$  is the full octahedral group where  $S_4$  ( $\supseteq \mathbb{Z}_2 \times \mathbb{Z}_2$ ) is the permutation group of order 24. We note that  $G_{K\Gamma}$  is nonsymmorphic in the sense that Eq. (12) is a non-split short exact sequence. For the purpose of MBQC in this work, we will only use the  $\mathbb{Z}_2 \times \mathbb{Z}_2$  subgroup in  $G_{K\Gamma}$ . How other nonsymmorphic symmetry operations beyond the  $\mathbb{Z}_2 \times \mathbb{Z}_2$  subgroup play a role in MBQC is an interesting and open question, which will be left for future investigations.

**Phase diagram.** We briefly describe the phase diagram of the model defined in Eq. (10) [35], using the parametrization  $K = \sin(\phi)$ ,  $\Gamma = \cos(\phi)$ ,  $g = g_y/g_x$ . There are four SPT phases in the phase diagram shown in Fig. 3 (a) [35], i.e., the EH, EH', OH, and OH' phases. Since the other three SPT phases are related to the EH phase by unitary transformations (for details, see Appendix B), it is enough to consider the EH phase, which is characterized by the following non-vanishing string order parameter in the  $|j - i| \rightarrow \infty$  limit in the rotated frame ( $\alpha \in \{x, y, z\}$ ) [35],

$$O^\alpha(2i + 1, 2j) = \langle \Pi_{k=2i+1}^{2j} 2S_k^\alpha \rangle. \quad (13)$$

We note that ‘‘EH’’ is ‘‘even-Haldane’’ for short, the name of which is chosen because of the fact that the phase is in the same SPT phase as the Haldane phase of the bilinear-biquadratic spin-1 chain [45–47].

Fig. 3 (b) shows the numerical values of the string order parameters  $O^\alpha(\frac{N}{2} + 1, N)$  ( $\alpha = x, z$ ) in the rotated frame as a function of  $\log(g)$  for an even-length chain ending with an  $x$ -bond on



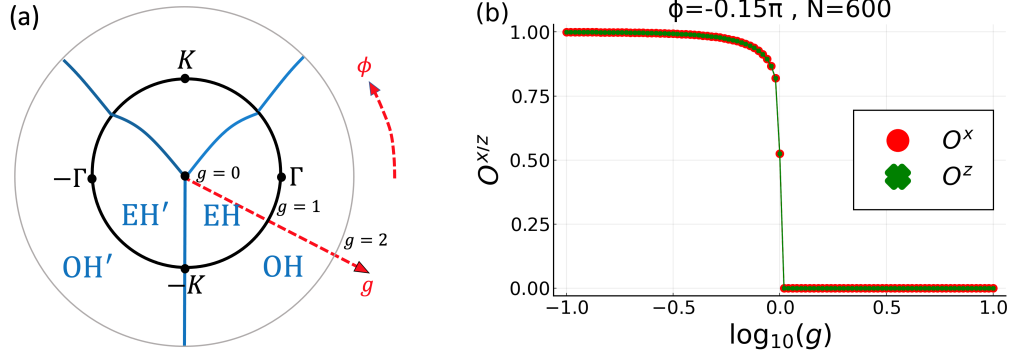


Figure 3: (a) Schematic plot of the phase diagram of the spin-1/2 bond-alternating Kitaev-Gamma chain, (b) string order parameters  $O^\alpha(\frac{N}{2} + 1, N)$  ( $\alpha = x, z$ ) as functions of  $\log(g)$  at  $\phi = -0.15\pi$ . In (a),  $K = \sin(\phi)$ ,  $\Gamma = \cos(\phi)$ , and  $g = g_y/g_x$ ;  $\phi$  and  $g$  are represented as azimuthal and radial coordinates, respectively; the center point, middle circle, and outer circle correspond to  $g = 0$ ,  $g = 1$ , and  $g = 2$ , respectively; the red dashed line is along the  $\phi = -0.15\pi$  radial direction; only the EH, EH', OH, OH' phases are shown, and the full phase diagram can be found in Ref. [35]. In (b), DMRG simulations are performed on open chains with system size  $N = 600$  ending with an  $x$ -bond on the right boundary.

the right boundary, where  $\phi$  is fixed to be  $-0.15\pi$  corresponding to the red dashed line in Fig. 3. Clearly, as can be seen from Fig. 3 (b), there is a phase transition at  $g = 1$ , separating the EH phase in the  $g < 1$  region from another phase (in fact, the OH phase) in the  $g > 1$  region. Discussions of the OH phase are included in Appendix B. The system in the EH phase has a non-degenerate ground state  $|\Phi_{K\Gamma}\rangle$ , with a spectral gap separating the ground state from the excited states. The state  $|\Phi_{K\Gamma}\rangle$  is short-range entangled with the  $\mathbb{Z}_2 \times \mathbb{Z}_2$  symmetries in Eq. (11), and can be used for MBQC purposes to be discussed in Sec. 4.5.2.

### 3.3.3 Cellular automaton states

In this section, we study MBQC resource states that are more entangled siblings of the 1D cluster state, and which have a larger symmetry group than the two previous examples. Indeed the purpose of this example is to illustrate that our main theorem applies beyond  $G = \mathbb{Z}_2 \times \mathbb{Z}_2$ .

The resource states discussed here, at the renormalization group fixed point, are generated by Clifford cellular automata, in  $\tau$  rounds of applying the transition function. The cluster state arises in this fashion, for  $\tau = 1$ . The larger  $\tau$  the larger the number of logical qubits that can be processed. It has recently been shown that universal MBQC resource states can be created in 1D in this fashion, when  $\tau$  is allowed to scale [48]. However, here we are content with a fixed value of  $\tau$ ,  $\tau = 2$ , yielding a model with two logical qubits. The symmetry group is  $(\mathbb{Z}_2)^4$ .

Specifically, we consider a quantum circuit with nearest neighbour interactions that takes the product state to the 1D cluster state of  $N$  qubits i.e.

$$U_N = \prod_{i=1}^{N-1} CZ_{i,i+1} \prod_{i=1}^N H_i. \quad (14)$$

where  $H = \frac{X+Z}{\sqrt{2}}$ , and  $CZ = |0\rangle\langle 0| \otimes I + |1\rangle\langle 1| \otimes Z$ . Now, this circuit is applied  $\tau$  times to the

product state  $\otimes_i |0\rangle_i$ , arriving at the resource states

$$|\Phi_\tau\rangle = (U_N)^\tau \left( \bigotimes_{i=1}^N |0\rangle_i \right). \quad (15)$$

The resources states  $|\Phi_\tau\rangle$  are capable of encoding  $\tau$  logical qubits on which MBQC can be performed. Such states can also be seen as fixed points belonging to different quantum phases with non-trivial SPT order.

In the remainder of this section, we focus on the case of  $\tau = 2$ , which suffices for our present purpose. We first note that  $|\Phi_2\rangle$  is a stabilizer state, constrained by the eigenvalue equations  $K_i|\Phi_2\rangle = |\Phi_2\rangle$ , for  $i = 1, \dots, N$ , with

$$K_i = Z_{i-2}X_{i-1}Z_iX_{i+1}Z_{i+2}, \quad i = 3, \dots, N-2$$

in the bulk, and

$$K_1 = X_2Z_3, \quad K_2 = X_1Z_2X_3Z_4, \quad K_{N-1} = Z_{N-3}X_{N-2}Z_{N-1}X_N, \quad K_N = Z_{N-2}X_{N-1}.$$

at the boundary. The above constraints specify the state uniquely, up to a global phase.

W.l.o.g we choose  $N = 6k + 4$ . The stabilizer is an Abelian group, with a subgroup

$$G_2 = \mathbb{Z}_2^4 \cong \left\langle \begin{array}{l} IZ(XIII XI) \dots XI, ZX(IIIX IX) \dots ZX, \\ XI(IIIX IXI) \dots IZ, ZI(IXIX II) \dots IX \end{array} \right\rangle. \quad (16)$$

$G_2$  is the symmetry group of interest. The  $\tau = 2$  automaton phase is the phase of  $G_2$ -symmetric states that contains the fixed point state.

The relevant string order parameters that capture the computational power of  $G_2$  symmetric states are given by

$$\begin{aligned} \sigma_1 &= \langle II \dots I(IIII Z)(XIII XI) \dots XI \rangle, \\ \sigma_2 &= \langle II \dots I(IIII ZX)(IIIX IX) \dots ZX \rangle, \\ \sigma_3 &= \langle II \dots I(IIIZ XI)(IIIX IXI) \dots IZ \rangle, \\ \sigma_4 &= \langle II \dots I(IIZX II)(IXIX II) \dots IX \rangle, \\ \sigma_5 &= \langle II \dots I(IZX III)(XIX III) \dots XZ \rangle, \\ \sigma_6 &= \langle II \dots I(ZXIII X)(IXIII X) \dots ZI \rangle, \end{aligned} \quad (17)$$

and expectation values of the all the non-trivial products of the operators involved in the first four string order parameters. For illustration, we consider a one-dimensional line in the phase diagram of  $\mathbb{Z}_2^4$ -symmetric states. Namely, of our interest are the ground states  $|\Phi_2(\alpha)\rangle$  of the Hamiltonian,

$$H(\alpha) = -\cos \alpha \sum_{i=1}^N K_i - \sin \alpha \sum_{i=3}^{N-2} X_i, \quad (18)$$

parametrized by an angle  $\alpha$ .

**Phase diagram.** When  $\alpha = 0$ , the ground state is the fixed point stabilizer state  $|\Phi_2\rangle$ . When  $\alpha = \pi/2$ , then the ground state is  $2^4$ -fold degenerate (due to the non-existence of magnetic fields at 4 boundary sites),  $|\Phi_2(\pi/2)\rangle = |\pm\rangle_1 |\pm\rangle_2 |\pm\rangle_3 \dots |\pm\rangle_{N-2} |\pm\rangle_{N-1} |\pm\rangle_N$ . At  $\alpha = \pi/4$  occurs a change-over from QCA-like states to trivial states. This change-over is marked by the string order parameters  $\sigma$  changing from non-zero to zero. See Fig. 4 for a plot of the order parameters in Eq. (17) as a function of  $\alpha$ .

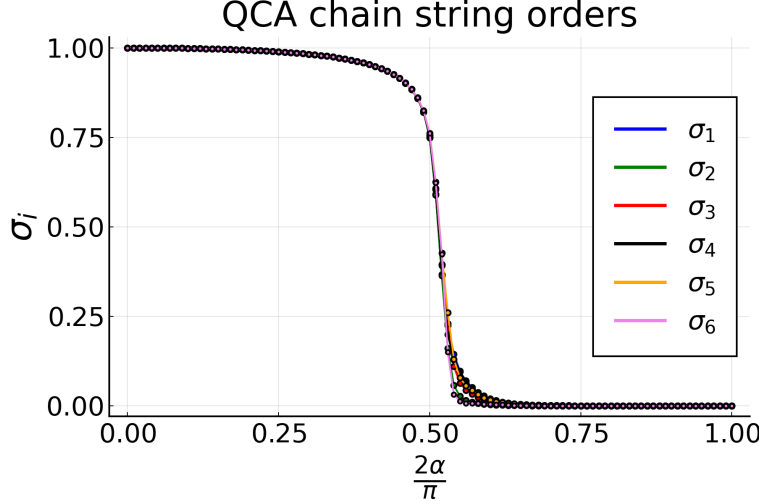


Figure 4: Order parameters  $\sigma_1, \sigma_2, \sigma_3, \sigma_4, \sigma_5, \sigma_6$  as a function  $\alpha$  for the cellular automaton states  $|\Phi_2(\alpha)\rangle$  on a chain length of  $N = 100$ . As before, they all start near the site  $N/4$  deep in the bulk.

### 3.3.4 The Ising chain

From the perspective of symmetry protected topological order, the Ising chain with transverse magnetic field is an odd case. The second cohomology group of its symmetry group  $\mathbb{Z}_2$  is the one-element group. Hence the only phase that exists in this model is the trivial phase, which has no computational power. The Ising model therefore is—from the quantum computational perspective—a non-example. The purpose of considering it here is to test how the new formalism handles it.

We consider the Ising Hamiltonian in a transverse magnetic field,

$$H = -g \cos \alpha \sum_{i=1}^{N-1} Z_i Z_{i+1} - g \sin \alpha \sum_{i=1}^N X_i. \quad (19)$$

This Hamiltonian is symmetric under the group  $\mathbb{Z}_2$  generated by

$$U(g_1) = X_1 X_2 \dots X_{N-1} X_N. \quad (20)$$

We are interested the ground state of this Hamiltonian, and if there is more than one, then we consider the eigenstates of the symmetry operator  $g_1$  in the ground state manifold.

## 4 MBQC on short-range entangled symmetric states

In this section, we state and prove our main result, Theorem 1 on the relation between string order and MBQC computational power. In Section 4.1 we make the necessary definitions; in Section 4.2 we describe the circuit model evolution simulated by MBQC; and in Section 4.3 we state the main theorem and explain how to use it. Section 4.4 gives the proof of the main theorem; and Section 4.5 applies it to the three examples introduced in Section 3.3.

## 4.1 Definitions

Here we define the notions required to parse our main result, Theorem 1 stated in Section 4.3. We begin by defining the pertaining representations of the symmetry group and their consistency conditions. After that, we define the MBQC measurement patterns and the string order parameters characterizing SPT in 1D systems, and specify the gate operations MBQC on the symmetric, short-range entangled states  $|\Phi\rangle$  can simulate.

### 4.1.1 Representations of the symmetry group

For the blocks  $i = 0, \dots, n + 1$  we define a number of representations of the symmetry group  $G$ . Namely, we have the linear representations

$$u_i(g), \forall g \in G, \quad \forall i = 0, \dots, n. \quad (21)$$

Beyond  $u$ , we have two projective representations per block,

$$\begin{aligned} v_{R,i}(g), \forall g \in G, \quad \forall i = 0, \dots, n, \\ v_{L,i}(g), \forall g \in G, \quad \forall i = 1, \dots, n + 1. \end{aligned} \quad (22)$$

For each block  $i = 1, \dots, n$ , we define a set  $\mathcal{G}_i \subseteq G$ . The sets  $\mathcal{G}_i$  appear for the first time in the constraints Eq. (25) and Eq. (26) below. As will become clear in the subsequent sections, they comprise the generators of unitary transformations that can be effected through measurement on any given block.

The above linear and projective representations satisfy the following consistency constraints.

1. The linear representation  $u_0$  on the left boundary is special. Namely, the symmetry group  $G$  has a maximal subgroup  $H$  with the property

$$[v_{R,0}(h), v_{R,0}(h')] = 0, \quad \forall h, h' \in H. \quad (23)$$

For this subgroup it holds that

$$u_0(h) = v_{R,0}(h), \quad \forall h \in H. \quad (24)$$

2. The commutation relations among the elements of the projective representation  $v_{L,n+1}(\cdot)$  are parametrized by a function  $\kappa : G \times G \rightarrow \mathbb{Z}_2$ ,

$$v_{L,n+1}(g)v_{L,n+1}(g') = (-1)^{\kappa(g,g')}v_{L,n+1}(g')v_{L,n+1}(g), \quad \forall g, g' \in G.$$

With this definition of  $\kappa$ , the following commutation relations hold

$$v_{R,i}(g)v_{R,i}(g') = (-1)^{\kappa(g,g')}v_{R,i}(g')v_{R,i}(g), \quad \forall g \in G, g' \in \mathcal{G}_i, i = 1, \dots, n, \quad (25)$$

and

$$[v_{L,i}(g), v_{R,i}(g')] = 0, \quad \forall g \in G, g' \in \mathcal{G}_i, \quad \forall i = 1, \dots, n, \quad (26)$$

3. On all blocks  $i = 1, \dots, n$ ,  $v_L$ ,  $v_R$  and  $u$  are related via

$$v_{L,i}(g)v_{R,i}(g) = u_i(g), \quad \forall g \in G, \quad \forall i = 1, \dots, n. \quad (27)$$

4. The linear representation  $U$  of  $G$  on the entire spin chain is given by

$$U(g) := v_{R,0}(g) \left( \bigotimes_{i=1}^n u_i(g) \right) v_{L,n+1}(g), \quad \forall g \in G. \quad (28)$$

The conditions Eqs. (24) – (28) need to be satisfied when applying the present formalism to examples. As discussed below in this section, Property 1 from the above list gives rise to initialization of the logical state, Properties 2 and 3 define the logical gate operations, and Property 4 characterizes the symmetry of the spin chain.

*Remark:* The function  $\kappa$  in the commutation relations Eq. (25) is independent of the block label  $i$ , and this is the only translation-invariant property we enforce. Yet, the restriction of the domain  $G \times \mathcal{G}_i$  may vary with the block label.

This concludes the definition of the relevant linear and projective representations of  $G$ . See Fig. 5 for a graphical display of the objects defined.

**Properties.** About the subsets  $\mathcal{G}_i \subset G$ , governing which logical rotations can be implemented at a given block  $i$ , we can say the following.

**Lemma 2** *For all blocks  $i = 1, \dots, n$ , the maximal sets  $\mathcal{G}_i$  are unique and are subgroups of  $G$ .*

*Proof of Lemma 2. (i) Uniqueness.* A set  $\mathcal{G}_i \subset G$  is maximal in  $G$  if it cannot be extended. The proof of uniqueness is by contradiction. Assume two distinct maximal sets exist,  $\mathcal{G}_i \neq \mathcal{G}'_i$ . Since all conditions on  $\mathcal{G}_i, \mathcal{G}'_i$ , namely Eq (25), Eq (26) are element-wise,  $\mathcal{G}_i \cup \mathcal{G}'_i$  is also a viable set  $\mathcal{G}$ . But  $\mathcal{G}_i, \mathcal{G}'_i \subsetneq \mathcal{G}_i \cup \mathcal{G}'_i$ , and hence  $\mathcal{G}_i, \mathcal{G}'_i$  are not maximal – contradiction. Thus the maximal set is unique.

*The maximal set  $\mathcal{G}_i$  is a subgroup.* It is easily verified that if  $g', g'' \in \mathcal{G}_i$  satisfy the constraints Eq. (25) and (26) on  $g'$ , then so does  $g'g''$ . Further,  $(g')^{-1} = g'$  for the present groups. Finally,  $g' = I$  also satisfies Eqs. (25), (26).  $\square$

#### 4.1.2 MBQC schemes and measurement patterns

The main result of this section, Theorem 1, attributes computational power to certain symmetric quantum states—without explicitly mentioning the measurement pattern that unlocks this computational power. But the proof of the theorem is constructive, and the measurement patterns used are the ones described below. We introduce those measurement patterns now, because they are a first application of the definitions made in the previous section.

**Independent constituents of MBQC measurement patterns.** All measurement patterns we consider have the same structure. They consist of various pieces of information, continuous and discrete. Some of those pieces are dependent, through the compatibility relations Eq. (24) – Eq. (28). We begin by listing the independent pieces. They are

1. The symmetry group  $G = (\mathbb{Z}_2)^m$ , for some  $m \in \mathbb{N}$ , and the required linear and projective representations of  $G$ ; namely
  - On the left boundary, i.e., block 0, the projective representation  $v_{R,0}(G)$ .
  - In the bulk, i.e., blocks  $i = 1, \dots, n$ , the linear representations  $u_i(G)$  and the projective representations  $v_{L,i}(G)$ .
  - On the right boundary, i.e., block  $n + 1$ , the projective representation  $v_{L,n+1}(G)$ .

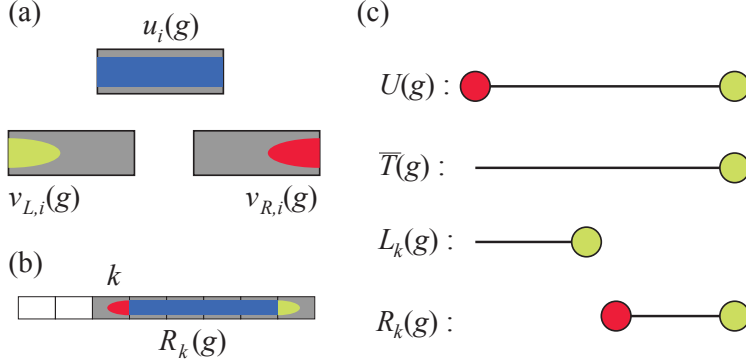


Figure 5: Representations of the symmetry group  $G$ . (a) For each site in the bulk, we use a linear representation  $u_i(G)$ , and two projective representations  $v_{L,i}(G)$ ,  $v_{R,i}(G)$ . The representation  $v_L$  “lives on the left” of the block, and connects to other blocks to the left of it.  $v_R$  connects to the blocks on the right. This is the reason for the naming. (b) An operator  $R_k(g)$  giving rise to a string order parameter. (c) Simpler graphical notation for some operators of interest. The coloured dots at the end points represent the projective representations  $v_L$  and  $v_R$  (same colouring as in (a) and (b)), and the line connecting them a string of linear representations  $u$ . Shown are the action  $U(G)$  of the symmetry  $G$  on the whole spin chain, the encoded Pauli operators  $\bar{T}(g)$ , the operators  $L_k(g)$  responsible for logical rotations evoked by measurement of the  $k$ -th block of spins, and  $R_k(g)$ , the operator giving rise to the string order parameter  $\sigma_k(g) = \langle R_k(g) \rangle$ .

2. The data that specifies any given quantum algorithm, namely

- For each block  $i = 1, \dots, n$  in the bulk, the basis of measurement specified by: (i) a rotation plane  $g_i \in \mathcal{G}_i$ , and (ii) a rotation angle  $\alpha_i \in [-\pi, \pi]$  (subject to the constraint that the angles can be non-zero only on blocks at least  $2\Delta$  apart).
- A subgroup  $H \subset G$ , specifying the logical initial state.
- A subgroup  $H' \subset G$ , specifying the logical readout.

3. The classical side processing relations to convert measurement record into computational output. There is one bit worth of measurement adjustment  $q_k$  for every block  $k = 1, \dots, n$ , and one bit of output  $o(h)$  for every group element  $h \in H'$ . The classical side-processing relations to obtain those from the measurement record  $s_i(g) \in \mathbb{Z}_2$ ,  $g \in G$ , are

$$\begin{aligned}
 q_k &= \sum_{i=0}^{k-1} s_i(g_k) \pmod{2}, \quad \forall k = 1, \dots, n, \\
 o(h) &= \sum_{i=0}^{n+1} s_i(h) \pmod{2}, \quad \forall h \in H'.
 \end{aligned}
 \tag{29}$$

The three items listed above live at various levels of generality. The measurement angles, measurement planes, and subgroups  $H$ ,  $H'$  in item 2 describe a given quantum algorithm within a fixed MBQC scheme. They do not describe MBQC schemes themselves. Item 3, the classical side processing relations, is at the opposite end of the spectrum. As we will prove, the classical side processing relations are of the same form Eq. (29) for *all* MBQC schemes in 1D. Hence they do not specify such MBQC schemes. The remaining entry in the list, item 1, contains the only independent information that discriminates between and hence characterizes MBQC schemes in 1D. It is the basis for a future classification of MBQC schemes with  $(\mathbb{Z}_2)^m$ -symmetry in 1D.

**Dependent constituents.** There are important parts of MBQC measurement patterns that are dependent through the constraints Eq. (24) – Eq. (28). Here we describe how to compute them.

1. For the bulk blocks,  $i = 1, \dots, n$  we compute the projective representations  $v_{R,i}(G)$  from  $v_{L,i}(G)$  and  $u_i(G)$  through Eq. (27).
2. On the left boundary, block 0, we compute  $u_0(G)$  as follows. On  $H \subset G$ ,  $u_0(\cdot)$  is obtained from  $v_{R,0}(G)$  through Eq. (24). On  $G \setminus H$ ,  $u_0(\cdot)$  is free to choose, subject to the constraint that  $u_0(G)$  is an Abelian group.
3. For the bulk blocks,  $i = 1, \dots, n$ , the groups  $\mathcal{G}_i \subset G$  of possible measurement planes are computed from the constraints Eq. (25) and (26).
4. The action of the symmetry group  $G$  on the spin chain as a whole is given by Eq. (28).

**Measurement procedure.** The measurements proceed from left to right, starting with block 0. The exception is block  $n + 1$  on the right boundary, whose basis is not adaptive and which therefore can be measured jointly with block 0 in the first measurement round. On the boundaries, the measured observables are

$$\begin{aligned} O_0(g) &= u_0(g), \quad \forall g \in G, \quad \text{for block 0,} \\ O_{n+1}(h) &= v_{L,n+1}(h), \quad \forall h \in H', \quad \text{for block } n + 1. \end{aligned} \quad (30)$$

In the bulk, the measured observables have a more complicated form. Namely, for any one  $g_k \in \mathcal{G}_k$  chosen for block  $k$ ,

$$O_k(g) = e^{-i(-1)^{q_k} \frac{\alpha_k}{2} v_{L,k}(g_k)} u_k(g) e^{i(-1)^{q_k} \frac{\alpha_k}{2} v_{L,k}(g_k)}, \quad \forall g \in G, \quad k = 1, \dots, n. \quad (31)$$

Therein,  $q_k \in \mathbb{Z}_2$  represents the adjustment of the measured observable according to measurement outcomes obtained elsewhere on the chain, as is usual in MBQC. Thus, in the bulk, the measurement in each block  $k$  is specified by  $q_k$ , a measurement angle  $\alpha_k$  and a logical rotation axis, given by the element  $g_k$  of the symmetry group  $G$ .

For any given  $k \leq n$ , the observables  $O_k(g)$  pairwise commute for all  $g \in G$ , and can thus be measured simultaneously. We denote the corresponding measurement outcomes by  $s_k(g) \in \mathbb{Z}_2$ . Since, by construction,  $O_k(g_1 g_2) = O_k(g_1) O_k(g_2)$ , it suffices to measure the observables corresponding to a set of generators of  $G$ . This completes the description of the measurement pattern.

It remains to connect this procedure to the logical processing it affects. We do this below in Sections 4.2 – 4.4.

### 4.1.3 The logical observables

Here, we introduce computationally relevant quantities and operators defined on the large Hilbert space  $\mathcal{H}$  in which the resource quantum state  $|\Phi\rangle$  lives. This leads up to the definition of string order parameters in Eq. (33) below, and to the sequence of observables

$$\{\bar{T}_t(g), \forall g \in G\}, \quad t = 0, \dots, n,$$

cf. Eq. (39) below. The observables  $\bar{T}_n(g)$ , for the maximum value  $n$  for  $t$ , give rise to the computational output.

Denote by  $L_k(g)$  and  $R_l(g)$  the operators

$$\begin{aligned} L_k(g) &:= \left( \bigotimes_{i=0}^{k-1} u_i(g) \right) v_{L,k}(g), & \forall g \in \mathcal{G}_i, \quad 1 \leq k \leq n, \\ R_l(g) &:= v_{R,l}(g) \left( \bigotimes_{j=l+1}^n u_j(g) \right) v_{L,n+1}(g), & \forall g \in \mathcal{G}_i, \quad 1 \leq l \leq n. \end{aligned} \quad (32)$$

The expectation values

$$\sigma_l(g) := \langle \Phi | R_l(g) | \Phi \rangle \quad (33)$$

are string order parameters. We shall see later in Corollary 1 that non-vanishing string order parameters provide computational power in MBQC. Eq. (40) is a precondition for the string order parameters to be non-zero.

We introduce the encoded Pauli operators

$$\bar{T}(g) := \left( \bigotimes_{i=0}^n u_i(g) \right) v_{L,n+1}(g), \quad \forall g \in G, \quad (34)$$

the unitary gates

$$V_k := \exp \left( -i \frac{\alpha_k}{2} L_k(g_k) \right), \quad -\pi \leq \alpha_k \leq \pi, \quad g_k \in \mathcal{G}_k. \quad (35)$$

The bar in the observables  $\bar{T}(g)$  in Eq. (34) denotes an encoding; i.e., we consider  $\bar{T}(g)$  an encoded version of  $v_{L,n+1}(g)$ , i.e.,  $\bar{T}(g) = \overline{v_{L,n+1}(g)}$ ,  $\forall g \in G$ . Per Eq. (34), the  $\{\bar{T}(g), g \in G\}$  and the  $\{v_{L,n+1}(g), g \in G\}$  have the same commutation relations, and, as the proof of Lemma 5 below will show, the evolution of the observables in Eq. (34) depends on those commutation relations only.

The observables  $\{\bar{T}_t(g), g \in G\}$  are now defined in a recursive fashion,

$$\bar{T}_t(g) = V_t^\dagger \bar{T}_{t-1}(g) V_t, \quad \forall g \in G, \quad \forall t = 1, \dots, n, \quad (36)$$

with the boundary condition

$$\bar{T}_0(g) = \bar{T}(g), \quad \forall g \in G. \quad (37)$$

Eq. (36) resembles evolution in the Heisenberg picture, but for now it is just a recursive definition of observables.

We also introduce a symbol for the accumulation of the gates in Eq. (35),

$$V_{\leq k} := V_k V_{k-1} \dots V_2 V_1. \quad (38)$$

Thus, the observables for “time”  $t = n$  are

$$\bar{T}_n(g) := V_{\leq n}^\dagger \bar{T}(g) V_{\leq n}, \quad \forall g \in G. \quad (39)$$

We later demonstrate that the measured eigenvalues of mutually commuting observables  $\bar{T}_n(g)$  represent the MBQC computational output. This concludes the definition of the logical observables.

**Properties.** We now establish a few elementary properties that follow from the above definitions. A first consequence of the above definitions is that

$$[R_k(g'), U(g)] = 0, \quad \forall g \in G, g' \in \mathcal{G}_k, k = 1, \dots, n. \quad (40)$$

This is a precondition for the above expectation values  $\sigma_l(g)$  to be non-zero.



Further, with Eq. (32) we find

$$\bar{T}(g) = L_i(g)R_i(g), \quad \forall g \in \mathcal{G}_i, \quad \forall i = 1, \dots, n, \quad (41)$$

and with Eq. (26) that

$$[L_i(g), R_i(g)] = 0, \quad \forall g \in \mathcal{G}_i, \quad \forall i = 1, \dots, n. \quad (42)$$

This means that for all  $i = 1, \dots, n$  and all  $g \in \mathcal{G}_i$ ,  $L_i(g)$ ,  $R_i(g)$  and  $\bar{T}(g)$  can simultaneously be chosen Hermitian; and this convention we adopt here. As a first consequence, the string order parameters  $\sigma_i(g)$  are all real.

For subsequent use in the proof of Theorem 1, we establish the following lemma.

**Lemma 3** *It holds that  $[R_k(g'), \bar{T}(g)] = 0$ , for all  $g \in G, g' \in \mathcal{G}_k, k = 1, \dots, n$ . Furthermore,  $[L_k(g'), \bar{T}(g)] = 0 \iff [\bar{T}(g'), \bar{T}(g)] = 0$ , for all  $g \in G, g' \in \mathcal{G}_k, k = 1, \dots, n$ .*

*Proof of Lemma 3.* For the first relation,

$$\begin{aligned} R_k(g')\bar{T}(g) &= (-1)^{\kappa(g, g') + \kappa(g, g')}\bar{T}(g)R_k(g') \\ &= \bar{T}(g)R_k(g'). \end{aligned}$$

Therein, we observe that contributions to the sign under commutation stem from blocks  $k$  and  $n + 1$ . In the equality we have used Eqs. (25), (26) and (27).

For the equivalence,  $0 = \bar{T}(g')\bar{T}(g) - \bar{T}(g)\bar{T}(g') = L_k(g')R_k(g')\bar{T}(g) - \bar{T}(g)L_k(g')R_k(g') = (L_k(g')\bar{T}(g) - \bar{T}(g)L_k(g'))R_k(g') \iff L_k(g')\bar{T}(g) - \bar{T}(g)L_k(g') = 0$ . Therein, the second equality on the l.h.s. of the equivalence is by Eq. (41), and the third equality by the first relation.  $\square$

With the definitions (28), (34) it further holds that

$$u_0^\dagger(g)\bar{T}(g) = v_{R,0}^\dagger(g)U(g), \quad \forall g \in G, \quad (43)$$

and specifically, with the condition Eq. (24),

$$\bar{T}(h) = U(h), \quad \forall h \in H. \quad (44)$$

With Eqs. (1) and (44), the resource state  $|\Phi\rangle$  is an eigenstate of all encoded Pauli operators  $\bar{T}(H)$ , namely

$$\bar{T}(h)|\Phi\rangle = (-1)^{\chi(h)}|\Phi\rangle, \quad \forall h \in H. \quad (45)$$

## 4.2 Evolution of the logical observables

*The logical initial state.* The MBQC resource states under consideration have the following property.

**Lemma 4** *Consider a short-range entangled state  $|\Phi\rangle$  of a spin-1/2 chain, symmetric under a group  $G = (\mathbb{Z}_2)^m$  with the symmetry represented as described above. Then it holds that*

$$\begin{aligned} \langle \bar{T}(g) \rangle_\Phi &= (-1)^{\chi(g)}, \quad \text{if } g \in H, \\ \langle \bar{T}(g) \rangle_\Phi &= 0, \quad \text{if } g \in G \setminus H. \end{aligned} \quad (46)$$

*Proof of Lemma 4.* For  $g \in H$ , Eq. (46) follows directly from Eq. (45). For  $g \in G \setminus H$ , since by assumption  $\bar{T}(H)$  is a maximal Abelian subgroup of  $\bar{T}(G)$ , exists an  $h \in H$  for which  $\bar{T}(g)$  and  $\bar{T}(h)$  anti-commute. With Eq. (45),  $\langle \Phi | \bar{T}(g) | \Phi \rangle = \langle \Phi | \bar{T}(h)^\dagger \bar{T}(g) \bar{T}(h) | \Phi \rangle = -\langle \Phi | \bar{T}(g) | \Phi \rangle$ , hence  $\langle \Phi | \bar{T}(g) | \Phi \rangle = 0$ .  $\square$

*The logical gates.* The gates defined in Eq. (35) have counterparts acting on the encoded logical qubits,

$$\bar{V}_k := \exp\left(-i\frac{\alpha_k}{2}\bar{T}(g_k)\right), \quad -\pi \leq \alpha_k \leq \pi, \quad g_k \in \mathcal{G}_k.$$

Based on those, we define the CPTP maps  $\bar{V}_k$  which, as we demonstrate below, are circuit model operations which can be simulated by MBQC on symmetric states  $|\Phi\rangle$ ,

$$\bar{V}_k := \frac{1 + \sigma_k(g_k)}{2}[\bar{V}_k] + \frac{1 - \sigma_k(g_k)}{2}[\bar{V}_k^\dagger]. \quad (47)$$

Herein, the brackets  $[\cdot]$  denote superoperators. The rotation angle  $\alpha_k$  and rotation axis specified by  $g_k$  are implicit. As before in Eq. (38), we define the concatenated operations  $\bar{V}_{\leq k} := \bar{V}_k \bar{V}_{k-1} \dots \bar{V}_1$ .

Now there are two important statements to make about the evolution of the above-introduced logical observables. First, the evolution of the expectation values  $\{\langle \bar{T}_t(g) \rangle_\Phi\}$  is closed. That is, the expectation values at any given time  $t$  depend only on the same expectation values at time  $t-1$ , in a linear fashion. This is a significant simplification, since there are only  $|G|$  operators  $\bar{T}_g(t)$ , i.e., a constant number independent of the chain length. The evolution of these few observables decouples from the exponentially many other observables defined on the Hilbert space  $\mathcal{H}$ .

Specifically, as we will prove below, we have the linear relations

$$\begin{pmatrix} \langle \bar{T}_t(g_1) \rangle_\Phi \\ \langle \bar{T}_t(g_2) \rangle_\Phi \\ \vdots \\ \langle \bar{T}_t(g_{|G|}) \rangle_\Phi \end{pmatrix} = [\mathcal{V}_t^\dagger] \begin{pmatrix} \langle \bar{T}_{t-1}(g_1) \rangle_\Phi \\ \langle \bar{T}_{t-1}(g_2) \rangle_\Phi \\ \vdots \\ \langle \bar{T}_{t-1}(g_{|G|}) \rangle_\Phi \end{pmatrix}, \quad \forall t = 1, \dots, n. \quad (48)$$

Therein, the  $|G| \times |G|$  matrix  $[\mathcal{V}_t^\dagger]$  depends on one measurement angle  $\alpha$  and a string order parameter as defined in Eq. (33). We have the following result.

**Lemma 5** *The measurement statistics resulting from action of the sequence of the logical CPTP maps  $\bar{V}_n \bar{V}_{n-1} \dots \bar{V}_2 \bar{V}_1$  on the resource state  $|\Phi\rangle$  with expectation values given by Eq. (46), followed by measurement of an Abelian subgroup of observables  $\bar{T}(H')$ ,  $H' \subset G$ , can be reproduced by measurement of the observables  $\bar{T}_n(h)$ ,  $h \in H'$ , on  $|\Phi\rangle$ ,*

$$\langle \Phi | \bar{T}_n(h) | \Phi \rangle = \text{Tr}(\bar{T}(h) \bar{V}_{\leq n}(|\Phi\rangle\langle\Phi|)). \quad (49)$$

Here, the l.h.s. represents the MBQC, and the r.h.s. represents the corresponding circuit simulation.

Recall that  $\bar{T}_n(h) := V_{\leq n}^\dagger \bar{T}(h) V_{\leq n}$ . On the r.h.s. of (49), the presence of  $\bar{V}_{\leq n}$  reveals the closedness of the evolution, cf. definition (47). Encoded logical operators are mapped to linear combinations of such operators under  $\bar{V}_{\leq n}$ , in accordance with Eq. (48).

When replacing  $V_{\leq n}$  by  $\bar{V}_{\leq n}$ , gaining closedness of the evolution has a flipside. Namely, we seem to lose unitarity. While the maps  $V_t$  are unitary, the CPTP maps  $\bar{V}_t$  are typically not. A priori, we are not interested in the noisy evolution afforded by CPTP maps; the goal is to implement unitary evolution. We will find, though, that this is not a problem—the unitary limit of interest can be recovered in a computationally efficient way; see Corollary 1 in Section 4.3.2.

The second important statement about the logical observables is that, although they are highly non-local objects, they can be measured in a block-local fashion. We have the following result.

**Lemma 6** *The measurement outcomes of the observables  $\bar{T}_n(h)$ ,  $h \in H'$ , with  $H' \subset G$  and  $v_{L,n+1}(H')$  an Abelian group, can be jointly inferred by block-local physical measurement and classical side processing.*

Lemmas 5 and 6 are proved in Section 4.4.

### 4.3 MBQC in the presence of symmetry

#### 4.3.1 Statement of the result

With the above notions introduced, we can now state the main result.

**Theorem 1** *Consider a short-range entangled state  $|\Phi\rangle$  of a spin-1/2 chain, symmetric under a group  $G = (\mathbb{Z}_2)^m$ ; and representations  $v_{L,i}, v_{R,i}$  (projective) and  $u_i$  (linear) of  $G$  satisfying Eqs. (24) – (28). Then, MBQC using block-local measurements on  $|\Phi\rangle$  can simulate quantum circuits consisting of (i) preparation of an initial state fully specified by the expectation values Eq. (46); (ii) the sequence of CPTP maps  $\mathcal{V}_{\leq n} = \mathcal{V}_n \dots \mathcal{V}_1$  given by Eq. (47), and (iii) final measurement of Pauli observables from an Abelian subgroup of  $\overline{T}(G)$ .*

#### 4.3.2 How to use Theorem 1

We now describe how to identify the computational power bestowed by the MBQC schemes described in Section 4.1.2 on a given resource state  $|\Phi\rangle$ .

**Computing the dependent constituents.** Proceed as described in Section 4.1.2. This yields in particular the definition of the string order parameters. Check which of the relevant string order parameters  $\sigma_k(g_k), g_k \in \mathcal{G}_k$ , are non-zero.

**Extracting the computational primitives.** For admissible measurement patterns, the computational primitives provided are identified through the following procedure.

1. The logical Pauli operators  $\overline{T}(g), g \in G$ , are computed through Eq. (34).
2. *Preparation:* With Lemma 4, the initial state  $|\Phi\rangle$  has expectation values of the logical observables as specified by Eq. (46).
3. *Logical measurement:* The final logical measurement is of the commuting observables  $\overline{T}(h), h \in H'$ . See Lemma 5.
4. *CPTP maps:* The CPTP maps  $\overline{\mathcal{V}}_k$  appearing in Theorem 1 are obtained as follows.
  - (a) Using Eq. (25) and (26), the groups  $\mathcal{G}_i$ , for  $i = 1, \dots, n$  are computed.
  - (b) There is one logical CPTP map for every element of any  $\mathcal{G}_k$ . Namely, if  $g_k \in \mathcal{G}_k$  then the logical map

$$\overline{\mathcal{V}}_k = \frac{1 + \sigma_k(g)}{2} \left[ e^{-i\frac{\alpha_k}{2}\overline{T}(g_k)} \right] + \frac{1 - \sigma_k(g)}{2} \left[ e^{i\frac{\alpha_k}{2}\overline{T}(g_k)} \right]$$

can be realized by measuring the observables Eq. (31) on block  $k$ .

**Computational power.** In the theorem statement it is not made explicit how much computational power is provided with the CPTP maps  $\mathcal{V}_k$ , and under which circumstances. Specifically, one might want to know which unitaries are reachable as limits of the CPTP maps. This is clarified by the following corollary.

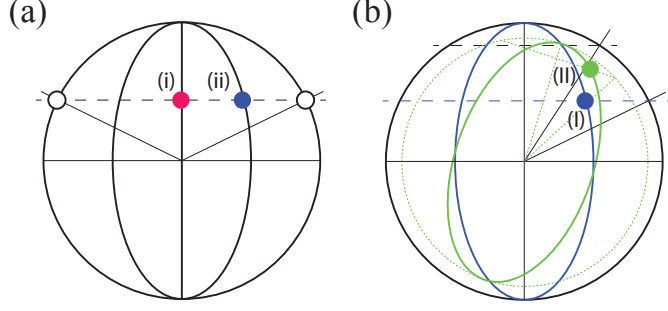


Figure 6: ‘Divide and conquer decoherence’ technique for MBQC-simulating unitary operations with high fidelity. The  $X/Y$ -equator of a Bloch sphere is shown. The implemented logical operation is a noisy rotation  $\mathcal{V}(\alpha)$  about the  $z$ -axis. (a) With Eq. (47), the noisy rotation  $\mathcal{V}(\alpha)$  is a probabilistic mixture of a unitary rotation  $U(\alpha)$  and  $U(-\alpha)$ . (i) When  $\sigma = 0$ , the mixture is 50/50, and no rotation occurs at all. (ii)  $\sigma = 1/2$ . The resulting operation amounts to rotation plus dephasing. (b) Splitting of one rotation into two of half the rotation angle. In the limit of small rotation angles, the total rotation angle is preserved, and the loss of purity is cut in half.

**Corollary 1** Consider a short-range entangled state  $|\Phi\rangle$  of a spin-1/2 chain, symmetric under a group  $G = (\mathbb{Z}_2)^m$ ; and (projective) representations  $v_{L,i}$ ,  $v_{R,i}$  and  $u_i$  of  $G$  satisfying Eqs. (24) – (28). Furthermore, assume that the string order parameters  $\sigma_k(g)$  are non-zero for at least  $N$  block locations  $k$ , spaced apart by a distance  $> 2\Delta$ , and  $|\sigma_k(g)| \geq \sigma > 0$  for all those locations. Then, the unitary gates

$$U_g(\alpha) = \exp\left(-i\frac{\alpha}{2}\bar{T}(g)\right) \quad (50)$$

can be implemented with error

$$\epsilon \leq \frac{\alpha^2}{N} \frac{1 - \sigma^2}{\sigma^2}. \quad (51)$$

The proof of Corollary 1 is given in Appendix A. The idea is to approximate the unitary  $U(\alpha)$  by the  $N$  fold iteration of the CPTP map  $\mathcal{V}(\alpha/\sigma N)$ . Each such step incurs an error proportional to  $\alpha^2/N^2$ ; hence the total error made in all  $N$  steps combined is proportional to  $1/N$ . It can be made arbitrarily small by increasing  $N$ . The technique of splitting one large rotation into a number of small rotations is illustrated in Fig. 6.

Corollary 1 tells us that, whatever the value of  $\sigma$ , as long as it is non-zero, any targeted approximation error  $\epsilon$  can be reached by a sufficiently large number of steps  $N$  into which the realization of  $U_g(\alpha)$  is subdivided. The smaller  $\sigma$ , the larger  $N$  needs to be.

The fundamental criterion for MBQC power on short-range entangled and symmetric states is whether the string order parameters are zero or non-zero. Vanishing string order parameters lead to no computational power, and non-vanishing order parameter imply computational power. As long as the order parameters are non-zero, the *kind* of computational power, i.e., the set of quantum gates realizable, is constant. However, the larger the value of the order parameters the more efficient the computation.

Further, while Eq. 50 describes the primitive gates that can be implemented, the entire set of gates is obtained by computing  $\mathcal{L}(\bar{T}) := \exp(-i\mathcal{A}(\bar{T}))$  where  $\mathcal{A}(\bar{T})$  is the algebra generated by the operators in  $\bar{T}$  under  $[\cdot, \cdot]/i$ . Namely, if we have two gates  $\exp(-i\alpha\bar{T}(g))$  and  $\exp(-i\alpha\bar{T}(g'))$  at

our disposal, we can also implement the unitary gate

$$\exp(-i\alpha\bar{T}(g))\exp(-i\alpha\bar{T}(g'))\exp(i\alpha\bar{T}(g))\exp(i\alpha\bar{T}(g'))\approx\exp(-(\alpha)^2[\bar{T}(g),\bar{T}(g')]).$$

Using the definition of  $\bar{T}(g)$  in Eq. 34, we conclude that the implementable gate set is isomorphic to  $\mathcal{L}(v_{L,n+1}) := \exp(-i\mathcal{A}(v_{L,n+1}))$ .

#### 4.4 Proof of Theorem 1

The proof of Theorem 1 is based on Lemmas 5 and 6 which were stated in Section 4.2. We prove them first. Recall that Lemma 5 establishes the closedness of the evolution of the logical observables  $\bar{T}_t(g)$ ,  $g \in G$ .

*Proof of Lemma 5.* There are two items to prove, namely (i) Eq. (49), and (ii) that the initial expectation values are given by Eq. (46).

(i). We prove Eq. (49) by way of two intermediate steps. As per the assumptions of the theorem, we consider a  $G$ -symmetric short-range entangled state  $|\Phi\rangle$  with entanglement range  $\Delta$ , and denote by  $k$  and  $l$  two blocks in the chain, such that  $l - k > 2\Delta$ . Further choose  $\alpha_{k+1}, \dots, \alpha_{l-1} = 0$ , i.e.,  $V_{k+1}, \dots, V_{l-1} = I$ . For easier book-keeping, we define sequences of states

$$|\Phi(k)\rangle := V_{\leq k}|\Phi\rangle.$$

Then it holds that

$$\langle\Phi(k)|\bar{T}(g)R_l(g')|\Phi(k)\rangle = \sigma_l(g')\langle\Phi(k)|\bar{T}(g)|\Phi(k)\rangle. \quad (52)$$

We use this to show that furthermore,

$$\langle\Phi(l)|\bar{T}(g)|\Phi(l)\rangle = \langle\Phi(k)|\bar{\mathcal{V}}_l^\dagger(\bar{T}(g))|\Phi(k)\rangle. \quad (53)$$

*Proof of Eq. (52).* For all  $g \in G$ , it holds that  $\bar{T}(g) = \bar{T}(g)|_{\{\leq k\}} \otimes \bar{T}(g)|_{\{> k\}}$ ,  $U(g) = U(g)|_{\{\leq k\}} \otimes U(g)|_{\{> k\}}$ ,  $\text{supp}(V_{\leq k}) \subseteq \{\leq k\}$ . Further, with Eq. (43),  $U(g)|_{\{> k\}} = \bar{T}(g)|_{\{> k\}}$ . Therefore,

$$\text{supp}\left(U(g)^\dagger V_{\leq k}^\dagger \bar{T}(g) V_{\leq k}\right) \subseteq \{\leq k\}. \quad (54)$$

Also,  $\text{supp}(R_l(g)) \subset \{> k\}$ , for all  $l > k$ , and therefore  $[V_{\leq k}, R_l(g')] = 0$ ,  $\forall g' \in G$ , whenever  $l > k$ . Thus we obtain

$$\begin{aligned} \langle\Phi(k)|\bar{T}(g)R_l(g')|\Phi(k)\rangle &= \langle\Phi|V_{\leq k}^\dagger\bar{T}(g)R_l(g')V_{\leq k}|\Phi\rangle \\ &= \langle\Phi|V_{\leq k}^\dagger\bar{T}(g)V_{\leq k}R_l(g')|\Phi\rangle \\ &= (-1)^{\chi(g)}\langle\Phi|\left(U(g)^\dagger V_{\leq k}^\dagger\bar{T}(g)V_{\leq k}\right)R_l(g')|\Phi\rangle \\ &= (-1)^{\chi(g)}\langle\Phi|U(g)^\dagger V_{\leq k}^\dagger\bar{T}(g)V_{\leq k}|\Phi\rangle\langle\Phi|R_l(g')|\Phi\rangle \\ &= \sigma_l(g')\langle\Phi|V_{\leq k}^\dagger\bar{T}(g)V_{\leq k}|\Phi\rangle \\ &= \sigma_l(g')\langle\Phi(k)|\bar{T}(g)|\Phi(k)\rangle. \end{aligned}$$

Therein, in the third equality we have used the symmetry property Eq. (1) of  $|\Phi\rangle$ . In the fourth equality we have used Eq. (54) and Lemma 1, and in the fifth equality Eq. (1) again. This proves Eq. (52), completing the first step.

*Proof of Eq. (53).*  $\bar{T}(g_l)$  and  $\bar{T}(g)$  are both Pauli operators, and so they either commute or anti-commute.

*Case I:*  $[\bar{T}(g_l), \bar{T}(g)] = 0$ . With Lemma 3 it follows that  $[L(g_l), \bar{T}(g)] = 0$ . The expectation value satisfies

$$\langle \Phi(l) | \bar{T}(g) | \Phi(l) \rangle = \langle \Phi(k) | V_l^\dagger \bar{T}(g) V_l | \Phi(k) \rangle = \langle \Phi(k) | \bar{T}(g) | \Phi(k) \rangle,$$

and so the observable  $\bar{T}(g)$  is not evolving. By the case assumption, this is matched by the operation  $\bar{\mathcal{V}}_l^\dagger$  at the logical level,

$$\langle \Phi(k) | \bar{\mathcal{V}}_l^\dagger (\bar{T}(g)) | \Phi(k) \rangle = \langle \Phi(k) | \bar{T}(g) | \Phi(k) \rangle. \quad (55)$$

This concludes Case I.

*Case II:*  $[\bar{T}(g_l), \bar{T}(g)] \neq 0$ . Since Pauli operators commute or anti-commute, with Lemma 3 it follows that  $\{L(g_l), \bar{T}(g)\} = 0$ . The expectation value of interest is

$$\begin{aligned} \langle \Phi(l) | \bar{T}(g) | \Phi(l) \rangle &= \langle \Phi(k) | V_l^\dagger \bar{T}(g) V_l | \Phi(k) \rangle \\ &= \cos(\alpha_l) \langle \Phi(k) | \bar{T}(g) | \Phi(k) \rangle - i \sin(\alpha_l) \langle \Phi(k) | \bar{T}(g) L_l(g_l) | \Phi(k) \rangle. \end{aligned}$$

We now focus on the expectation value in the term  $\sim \sin(\alpha_l)$ ,

$$\begin{aligned} \langle \Phi(k) | \bar{T}(g) L_l(g_l) | \Phi(k) \rangle &= \langle \Phi(k) | \bar{T}(g) \bar{T}(g_l) R_l(g_l) | \Phi(k) \rangle \\ &= \langle \Phi | V_{\leq k}^\dagger \bar{T}(g) \bar{T}(g_l) V_{\leq k} R_l(g_l) | \Phi \rangle \\ &= (-1)^{\chi(gg_l)} \langle \Phi | \left( U(gg_l)^\dagger V_{\leq k}^\dagger \bar{T}(g) \bar{T}(g_l) V_{\leq k} \right) R_l(g_l) | \Phi \rangle \\ &= (-1)^{\chi(gg_l)} \langle \Phi | U(gg_l)^\dagger V_{\leq k}^\dagger \bar{T}(g) \bar{T}(g_l) V_{\leq k} | \Phi \rangle \langle \Phi | R_l(g_l) | \Phi \rangle \\ &= \sigma_l(g_l) \langle \Phi(k) | \bar{T}(g) \bar{T}(g_l) | \Phi(k) \rangle. \end{aligned}$$

Herein, in the fourth line we have used that  $\bar{T}(g) \bar{T}(g_l) \propto \bar{T}(gg_l)$ , then Eq. (54) for  $gg_l \in G$ , and finally Lemma 1. We thus arrive at

$$\langle \Phi(l) | \bar{T}(g) | \Phi(l) \rangle = \cos(\alpha_l) \langle \Phi(k) | \bar{T}(g) | \Phi(k) \rangle - i \sin(\alpha_l) \sigma_l(g_l) \langle \Phi(k) | \bar{T}(g) \bar{T}(g_l) | \Phi(k) \rangle.$$

The above may be rewritten as

$$\langle \Phi(l) | \bar{T}(g) | \Phi(l) \rangle = \frac{1 + \sigma_l(g_l)}{2} \langle \Phi(k) | \bar{\mathcal{V}}_l^\dagger \bar{T}(g) \bar{\mathcal{V}}_l | \Phi(k) \rangle + \frac{1 - \sigma_l(g_l)}{2} \langle \Phi(k) | \bar{\mathcal{V}}_l \bar{T}(g) \bar{\mathcal{V}}_l^\dagger | \Phi(k) \rangle. \quad (56)$$

This concludes Case II.

With Eqs. (55) and (56), recalling the definition of  $\bar{\mathcal{V}}_k$  from Eq. (47), in both the commuting and the anti-commuting case we find

$$\langle \Phi(l) | \bar{T}(g) | \Phi(l) \rangle = \langle \Phi(k) | \bar{\mathcal{V}}_l^\dagger (\bar{T}(g)) | \Phi(k) \rangle,$$

establishing Eq. (53). This completes the second step.

We now apply Eq. (53) recursively. In accordance with the assumptions of the theorem, consider a sequence of unitaries  $V_k$  where non-zero rotation angles  $\alpha_k$  are sparse. Namely, they only occur at locations  $1 = k_1, k_2, \dots, k_{\max} = n$ , with the spatial separations  $k_{i+1} - k_i > 2\Delta, \forall i$ . Under these conditions we can apply Eq. (53), and obtain

$$\langle \Phi | V_{\leq n}^\dagger \bar{T}(g) V_{\leq n} | \Phi \rangle = \langle \Phi | \bar{\mathcal{V}}_{\leq n}^\dagger (\bar{T}(g)) | \Phi \rangle, \quad \forall g \in G.$$

Using the cyclicity of trace on the r.h.s., we transform the above into

$$\langle \Phi | V_{\leq n}^\dagger \bar{T}(g) V_{\leq n} | \Phi \rangle = \text{Tr} (\bar{T}(g) \bar{\mathcal{V}}_{\leq n} (|\Phi\rangle\langle\Phi|)), \quad \forall g \in G.$$

This establishes Eq. (49).

(ii). Eq. (49), which we have proved above, on the r.h.s. has the state  $|\Phi\rangle\langle\Phi|$  as the initial state of the evolution. Its relevant expectation values have been provided by Eq. (46) in Lemma 4.  $\square$

We recall that Lemma 6 states that the observables  $\bar{T}_n(g)$  can be measured in a local fashion.

*Proof of Lemma 6.* The observables of interest are  $\bar{T}_n(h)$ ,  $\forall h \in H$ , as defined in Eq. (39). Using the commutation relations

$$[L_k(g_k), u_l(g)] = 0, \quad \forall g_k, g \in G, \text{ whenever } k \neq l \leq n, \quad (57)$$

and defining the unitaries (mind the ordering),

$$\tilde{V}_k := V_{\leq k-1}^\dagger V_k V_{\leq k-1}, \quad \text{for } k \leq n,$$

we may rewrite the observables  $\bar{T}_n(h)$  as follows,

$$\begin{aligned} \bar{T}_n(h) &= V_{\leq n}^\dagger (u_0(h)u_1(h) \dots u_n(h)v_{L,n+1}(h)) V_{\leq n} \\ &= u_0(h) \left( V_{\leq 1}^\dagger u_1(h) V_{\leq 1} \right) \dots \left( V_{\leq k}^\dagger u_k(h) V_{\leq k} \right) \dots \left( V_{\leq n}^\dagger u_n(h) V_{\leq n} \right) v_{L,n+1}(h), \end{aligned}$$

and thus,

$$\bar{T}_n(h) = u_0(h) \left( \tilde{V}_1^\dagger u_1(h) \tilde{V}_1 \right) \dots \left( \tilde{V}_k^\dagger u_k(h) \tilde{V}_k \right) \dots \left( \tilde{V}_n^\dagger u_n(h) \tilde{V}_n \right) v_{L,n+1}(h). \quad (58)$$

We now show by induction that all terms in the above product—the observables  $\tilde{V}_k^\dagger u_k(h) \tilde{V}_k$ —can be measured sequentially in a local fashion. To this end, we now rewrite  $\tilde{V}_k$  as introduced above,

$$\begin{aligned} \tilde{V}_k &= V_{\leq k-1}^\dagger \exp \left( -i \frac{\alpha_k}{2} u_0(g_k) \dots u_{k-1}(g_k) v_{L,k}(g_k) \right) V_{\leq k-1} \\ &= \exp \left( -i \frac{\alpha_k}{2} V_{\leq k-1}^\dagger (u_0(g_k) \dots u_{k-1}(g_k)) V_{\leq k-1} v_{L,k}(g_k) \right) \\ &= \exp \left( -i \frac{\alpha_k}{2} u_0(g_k) \dots \left( V_{\leq l}^\dagger u_l(g_k) V_{\leq l} \right) \dots \left( V_{\leq k-1}^\dagger u_{k-1}(g_k) V_{\leq k-1} \right) v_{L,k}(g_k) \right) \\ &= \exp \left( -i \frac{\alpha_k}{2} u_0(g_k) \dots \left( \tilde{V}_l^\dagger u_l(g_k) \tilde{V}_l \right) \dots \left( \tilde{V}_{k-1}^\dagger u_{k-1}(g_k) \tilde{V}_{k-1} \right) v_{L,k}(g_k) \right). \end{aligned} \quad (59)$$

The induction assumption is: for  $l = 1 \dots k-1$ , the observables  $\tilde{V}_l^\dagger u_l(g) \tilde{V}_l$  and  $u_0(g)$  can be jointly measured, for all  $g \in G$ . The claim of the induction is: As long as  $k \leq n$ , for  $l = 1 \dots k$ , the observables  $\tilde{V}_l^\dagger u_l(g) \tilde{V}_l$  and  $u_0(g)$ , for all  $g \in G$ , can be jointly measured.

For  $l = 0 \dots k-1$  the claim of the induction equals the assumption, and so we only need to discuss the observables  $\tilde{V}_k^\dagger u_k(g) \tilde{V}_k$ ,  $\forall g \in G$ . With Eq. (59), under the induction assumption it holds that,

$$\begin{aligned} \tilde{V}_k &\cong \exp \left( -i \frac{\alpha_k}{2} (-1)^{s_0(g_k)} \dots (-1)^{s_l(g_k)} \dots (-1)^{s_{k-1}(g_k)} v_{L,k}(g_k) \right) \\ &= \exp \left( -i \frac{\alpha_k}{2} (-1)^{q_k} v_{L,k}(g_k) \right), \end{aligned}$$

where in the second line we have used the classical side processing relation Eq. (29).

Thus,

$$\tilde{V}_k^\dagger u_k(g) \tilde{V}_k \cong O_k(g), \quad \forall g \in G.$$

The observables  $O_k(g)$ ,  $\forall g \in G$ , pairwise commute; and they also commute with all earlier observables  $O_l(g)$ , for  $l < k$ . The observables  $\tilde{V}_k^\dagger u_k(g) \tilde{V}_k$  can thus all be jointly measured, in addition to the already performed measurements. This concludes the induction step.

The induction begins at  $k = 1$ . We measure the commuting observables  $u_0(g), \forall g \in G$ , on block 0. Further we have

$$\begin{aligned}\tilde{V}_1 &= V_1 \\ &= \exp\left(-i\frac{\alpha_1}{2}u_0(g_1)v_{L,1}(g_1)\right) \\ &\cong \exp\left(-i\frac{\alpha_1}{2}(-1)^{s_0(g_1)}v_{L,1}(g_1)\right) \\ &= \exp\left(-i\frac{\alpha_1}{2}(-1)^{q_1}v_{L,1}(g_1)\right).\end{aligned}$$

Therefore,  $\tilde{V}_1^\dagger u_1(g)\tilde{V}_1 \cong O_1(g), \forall g \in G$ , can be jointly measured. The induction assumption holds for  $k = 1$ . This concludes the induction argument.

We have thus reduced the measurement of  $\bar{T}_n(g)$ , for all  $g \in G$ , to the last term in the expansion Eq. (58),  $v_{L,n+1}(g)$ . In general, not all these terms can be measured jointly for they form a projective representation of  $G$ . However, we can measure any Abelian subgroup of  $v_{L,n+1}(G)$ , which we denote by  $H'$ . Using the classical processing relations Eq. (29), we can jointly infer the values  $\bar{T}_n(h), \forall h \in H'$ , by block-local measurement.  $\square$

We are now ready to prove the main theorem.

*Proof of Theorem 1.* Lemma 5 relates the evolution described in the theorem to the expectation values  $\langle \Phi | \bar{T}_n(h) | \Phi \rangle$ , for all  $h \in H'$ , cf. Eq. (49). Lemma 6 shows how to measure the observables  $\bar{T}_n(h), h \in H$ , in a block-local fashion.  $\square$

## 4.5 Examples

In this first round of applying Theorem 1 to our examples, we make the simplest choice for the representations, which will lead to  $\mathcal{G}_i = G, \forall i = 1, \dots, n$ . For the cluster case, where previous results [7], [15, 16] exist, this will produce a block structure (blocks of size 2) compatible with those earlier results. We will return to the question of obtaining smaller blocks, specifically blocks of size one, in Section 5.

### 4.5.1 The cluster chain

We choose blocks  $i = 1, \dots, n$  of size 2, on the left boundary, for  $i = 0$  a block of size 2, and on the right boundary, for  $i = n + 1$ , a block of size 1. In this way, we obtain a chain of odd length which is the default for the cluster chain.

As discussed in Section 4.3.2, the measurement pattern is specified by the linear representations  $u_i$  and the projective representations  $v_{L,i}$ . In the bulk, they are

$$\begin{aligned}u_i(g_{01}) &= IX, & u_i(g_{10}) &= XI, \\ v_{L,i}(g_{01}) &= ZI, & v_{L,i}(g_{10}) &= XZ,\end{aligned}\tag{60}$$

The representations  $u_0, v_{R,0}$  on the left boundary are

$$\begin{aligned}u_0(g_{01}) &= IX, & u_0(g_{10}) &= XI, \\ v_{R,0}(g_{01}) &= ZX, & v_{R,0}(g_{10}) &= XI,\end{aligned}\tag{61}$$

The representation  $v_{L,n+1}$  on the right boundary is

$$v_{L,n+1}(g_{01}) = Z, \quad v_{L,n+1}(g_{10}) = X.\tag{62}$$

This concludes the specification of the measurement pattern, and we now unpack it.

With Eq. (27) we find that in the bulk

$$v_{R,i}(g_{01}) = ZX, \quad v_{R,i}(g_{10}) = IZ.\tag{63}$$



With Eq. (24) and Eq. (61), we find that  $H = \langle g_{10} \rangle$ . The representations are independent of the block label in the bulk, and therefore Eq. (25) is satisfied for  $i = 1, \dots, n$ . Comparing Eqs. (60) and (61), we find that the commutation relations for  $v_R$  are the same on block 0.

From Eqs. (25) and (26), we compute the sets  $\mathcal{G}_i$ , finding

$$\mathcal{G}_i = G, \quad \forall i = 1, \dots, n. \quad (64)$$

Inserting Eqs. (60), (61), (62) into Eq. (28) produces

$$g_{01} \cong ZXIXIXIXI\dots IXZ, \quad g_{10} \cong XIXIXIX\dots IZ. \quad (65)$$

All constraints are verified, and Theorem 1 can be applied.

With Eq. (34), (64) and Corollary 1, we find that we can implement rotations of form

$$e^{i\alpha X}, e^{i\beta Z}, e^{i\gamma Y}, \quad (66)$$

and hence all unitaries in  $SU(2)$ , by block-local measurements of block-size 2.

#### 4.5.2 The Kitaev-Gamma chain

For the spin-1/2 bond-alternating Kitaev-Gamma chain, we choose blocks  $i = 1, 2, \dots, n$  of size 2; on the left boundary  $i = 0$  of block size 1; and on the right boundary  $i = n + 1$  of block size 1. Hence the chain length is chosen as  $2n + 2 \in \mathbb{Z}$  in this case. We will work in the six-sublattice rotated frame in this subsection.

Next we specify the linear representations  $u_i$  and the projective representations  $v_{L,i}, v_{R,i}$  of the  $\mathbb{Z}_2 \times \mathbb{Z}_2 = \{1, R(\hat{x}, \pi), R(\hat{y}, \pi), R(\hat{z}, \pi)\}$  group. Since the group can be decomposed as  $\langle R(\hat{x}, \pi) \rangle \times \langle R(\hat{z}, \pi) \rangle$ , it is enough to specify the representations of the two generators. In the bulk,  $u_i$  and  $v_{L,i}$  are ( $i = 1, \dots, n$ )

$$\begin{aligned} u_i(R(\hat{x}, \pi)) &= XX, & u_i(R(\hat{z}, \pi)) &= ZZ, \\ v_{L,i}(R(\hat{x}, \pi)) &= XI, & v_{L,i}(R(\hat{z}, \pi)) &= ZI. \end{aligned} \quad (67)$$

Using Eq. (27), we find that in the bulk,

$$v_{R,i}(R(\hat{x}, \pi)) = IX, \quad v_{R,i}(R(\hat{z}, \pi)) = IZ. \quad (68)$$

On the left boundary, the projective representation  $v_{R,0}$  is

$$v_{R,0}(R(\hat{x}, \pi)) = X, \quad v_{R,0}(R(\hat{z}, \pi)) = Z. \quad (69)$$

Since except the identity element, the other three elements in the  $\mathbb{Z}_2 \times \mathbb{Z}_2$  group anti-commute in  $v_{R,0}$ , the maximal abelian subgroup in  $v_{R,0}$  can at most be  $\mathbb{Z}_2$ . As a result,  $H$  in Eq. (23) can be chosen as  $\langle R(\hat{x}, \pi) \rangle$ . Defining the linear representation  $u_0$  to be

$$u_0(R(\hat{x}, \pi)) = X, \quad u_0(R(\hat{z}, \pi)) = I, \quad (70)$$

it can be verified that Eq. (24) is satisfied.

Finally, on the right boundary,  $v_{L,n+1}$  is

$$v_{L,n+1}(R(\hat{x}, \pi)) = X, \quad v_{L,n+1}(R(\hat{z}, \pi)) = Z. \quad (71)$$

The linear representation  $U$  of the  $\mathbb{Z}_2 \times \mathbb{Z}_2$  group on the whole chain can be obtained from Eq. (28) as

$$U(R(\hat{x}, \pi)) = \prod_{i=0}^{n+1} X_i, \quad U(R(\hat{z}, \pi)) = \prod_{i=0}^{n+1} Z_i, \quad (72)$$

which is the same as Eq. (11). Furthermore, the group  $\mathcal{G}_i$  ( $i = 1, 2, \dots, n$ ) is just the full  $\mathbb{Z}_2 \times \mathbb{Z}_2$  group, since Eqs. (25,26) can be verified using Eqs. (67,68). Then it can be checked that the assumptions in Sec. 4.1.1 are all satisfied. Therefore, from Corollary 1, we find that we can implement rotations of form  $e^{i\alpha X}$ ,  $e^{i\beta Z}$ ,  $e^{i\gamma Y}$ , and hence all unitary operations in  $SU(2)$ , by block-local measurements of block-size 2.

Two comments are in order. First, in addition to the Kitaev-Gamma model, the MBQC procedure is applicable to 1D bond-alternating spin-1/2 XXZ and XYZ models as well, since these models are invariant under the  $\{1, R(\hat{x}, \pi), R(\hat{y}, \pi), R(\hat{z}, \pi)\} \cong \mathbb{Z}_2 \times \mathbb{Z}_2$  symmetry group and the constructions of the representations  $u_i$ ,  $v_{L,i}$  and  $v_{R,i}$  are the same as the Kitaev-Gamma model. Second, the Hamiltonian of the bond-alternating Kitaev-Gamma model in the  $U_6$  frame does not have a two-site translation invariance, and instead, the periodicity is six. However, this does not stop us from performing block-size-two measurements as translation invariance is not required in the present MBQC formalism.

### 4.5.3 Cellular automaton states

We choose blocks  $i = 1, \dots, n$  of size 6, for  $i = 0$  a block of size 2, and on the right boundary, for  $i = n + 1$ , a block of size 2. Thus the natural chain length of choice for the  $\tau = 2$  automaton phase is  $6n + 4$ .

As discussed in Section 4.3.2, the measurement pattern is specified by the linear representations  $u_i$  and the projective representations  $v_{L,i}$ . In the bulk,  $u_i$  is generated by

$$\begin{aligned} u_i(g_1) &= XIII XI, & u_i(g_2) &= III XI, \\ u_i(g_3) &= IIX IXI, & u_i(g_4) &= IX IXI, \end{aligned} \quad (73)$$

and  $v_i$  is generated by

$$\begin{aligned} v_{L,i}(g_1) &= XIII XZ, & v_{L,i}(g_2) &= III XZI, \\ v_{L,i}(g_3) &= IIX ZII, & v_{L,i}(g_4) &= IX ZIII. \end{aligned} \quad (74)$$

The representation  $u_0$  on the left boundary is given by

$$u_0(g_1) = IZ, \quad u_0(g_2) = II, \quad u_0(g_3) = XI, \quad u_0(g_4) = II. \quad (75)$$

The representation  $v_{L,n+1}$  on the right boundary is

$$v_{L,n+1}(g_1) = XI, \quad v_{L,n+1}(g_2) = ZX, \quad v_{L,n+1}(g_3) = IZ, \quad v_{L,n+1}(g_4) = IX, \quad (76)$$

and  $v_{R,0}$  on the left boundary is

$$v_{R,0}(g_1) = IZ, \quad v_{R,0}(g_2) = ZX, \quad v_{R,0}(g_3) = XI, \quad v_{R,0}(g_4) = ZI. \quad (77)$$

This concludes the specification of the measurement pattern, and we now unpack it.

With Eq. (27) we find that in the bulk

$$v_{R,i}(g_1) = IIII Z, \quad v_{R,i}(g_2) = IIII ZX, \quad v_{R,i}(g_3) = IIII ZXI, \quad v_{R,i}(g_4) = IIII ZXI. \quad (78)$$

With Eq. (24) and Eq. (75), we find that  $H = \langle g_1, g_3 \rangle$ . The representations are faithful and independent of the block label in the bulk.

From Eqs. (25) and (26), we compute the sets  $\mathcal{G}_i$ , finding

$$\mathcal{G}_i = G, \quad \forall i = 1, \dots, n. \quad (79)$$

Inserting Eqs. (77), (73), (76) into Eq. (28) produces

$$\begin{aligned} g_1 &\cong IZ(XIII XI) \dots XI, & g_2 &\cong ZX(III XIX) \dots ZX, \\ g_3 &\cong XI(II XIX I) \dots IZ, & g_4 &\cong ZI(IX IX II) \dots IX. \end{aligned} \quad (80)$$

All constraints are verified, and Theorem 1 can be applied.

With Eq. (34), (79) and Corollary 1, we find that we can implement rotations of form

$$e^{i\alpha_{ij}\sigma^i\sigma^j}, \text{ for } i, j = 0, 1, 2, 3 \quad (81)$$

where  $\sigma^0 \equiv I, \sigma^1 \equiv X, \sigma^2 \equiv Y, \sigma^3 \equiv Z$ , and hence all unitaries in  $SU(4)$ , by block-local measurements of block-size 6.

#### 4.5.4 The Ising chain

SPT analysis implies the absence of uniform MBQC computational power in the ground state of the infinite Ising chain with transverse magnetic field. We now show how the present formalism produces a matching result for all finite system sizes. In fact, the argument below applies to any system with  $\mathbb{Z}_2$  symmetry, implemented in a manner consistent with Eqs. (23)–(27). The Ising chain is only an example thereof, serving as illustration.

There are two choices for each  $\mathcal{G}_i$ , (i)  $\mathcal{G}_i = \{0\}$ , and (ii)  $\mathcal{G}_i = \mathbb{Z}_2$ .

Case (i),  $\mathcal{G}_i = \{0\}$ . There is no non-trivial computation. With Eq. (83), the measured observables  $O_i(g)$ , defined in Eq. (31), remain  $O_i(g) = u_i(g)$ , irrespective of the measurement angle  $\alpha_i$ , and the resulting logical CPTP map, defined in Eq. (47), is  $\bar{\mathcal{V}}_i = [I]$ .

Case (ii),  $\mathcal{G}_i = \mathbb{Z}_2$ .  $\mathcal{G}_i$  now has one additional element,  $g_1$ . Inspecting Eq. (26), we find

$$[v_{L,i}(g), v_{R,i}(g')] = 0, \quad \forall g, g' = \mathbb{Z}_2. \quad (82)$$

Further,  $\mathbb{Z}_2$  has only linear representations, hence  $[v_{L,i}(g), v_{L,i}(g')] = 0, \quad \forall g, g' = \mathbb{Z}_2$ . Therefore, with Eq. (27), Eq. (82) implies

$$[v_{L,i}(g), u_i(g')] = 0, \quad \forall g, g' = \mathbb{Z}_2. \quad (83)$$

With Eq. (83), the measured observables  $O_i(g)$  given by Eq. (31) are  $O_i(g) \equiv u_i(g)$ , irrespective of the measurement angle  $\alpha_i$ . Hence there is no way to imprint a non-trivial computation on the resource state.

Furthermore, for any block  $i$  the only (potentially) non-trivial operation is

$$\bar{\mathcal{V}}_i(g_1) = \frac{1 + \sigma_i(g_1)}{2} [\exp(-i\alpha_i/2\bar{T}(g_1))] + \frac{1 - \sigma_i(g_1)}{2} [\exp(i\alpha_i/2\bar{T}(g_1))]. \quad (84)$$

The only non-trivial observable available for measurement is  $\bar{T}(g_1)$ . Thus, all evolution according to Eq. (84) can be absorbed in the measurement, leaving it unchanged.

Further, with the maximality of  $H$ , we find  $H = \mathbb{Z}_2$ . Therefore, with Lemma 4, the initial logical state satisfies  $\langle \bar{T}(g_1) \rangle = (-1)^{\chi(g_1)}$ . Hence the only circuit that can be implemented is preparing an eigenstate of  $\bar{T}(g_1)$  and measuring the corresponding eigenvalue  $(-1)^{\chi(g_1)}$ . Again, no non-trivial computation arises.

### 4.5.5 Approaching trivial SPT phases

To conclude Section 4.5, we discuss an aspect common to the first three of the above examples, which interpolate between a computationally useful and a computationally trivial regime. Of our interest are parameter regimes where the thermodynamic limit is a trivial SPT phase. For such finite systems, the string order parameter may be non-zero for any given system size, providing some computational power. However, as we demonstrate below, the power decreases to zero with increasing system size.

If the string order parameter is zero in the thermodynamic limit, it decays exponentially in finite size systems [26, 27], namely, there exist  $D \in \mathbb{Z}$  and  $\xi > 0$ , such that when  $d > D$ , we have  $|\sigma_k(g)| \leq e^{-d/\xi}$ , where  $d$  is the distance between block  $k$  and the right boundary. Suppose the angle  $\alpha$  is split into  $N$  pieces as in Corollary 1. When  $N > D/(2\Delta)$ , there is an overflow of the split rotations into the exponentially decaying region. The MBQC rotation angle that can be implemented in the exponentially decaying region is bounded from above by

$$\sum_{n=0}^{\infty} \frac{\alpha}{N} e^{-(D+2n\Delta)/\xi} = \frac{1}{N} \frac{\alpha e^{-D/\xi}}{1 - e^{-2\Delta/\xi}}, \quad (85)$$

where the upper limit of the sum is set as infinity since we are only interested in an upper bound. In the region within a  $D$  distance from the right boundary, the MBQC rotation angle is upper bounded by  $\frac{\alpha D \sigma_{max}}{2N\Delta}$ , where  $\sigma_{max} = \sup\{|\sigma_k(g)|\}_{k,g}$ . Combining the two regions, the overall implemented rotation angle is on order of  $1/N$ , which approaches zero when  $N$  becomes large, equivalent to saying that the system size is increasingly large since it is bounded from below by  $2N\Delta$ . Therefore, finite unitary gate operations cannot be approximated to arbitrary high accuracies in this case, meaning MBQC power is lost in trivial SPT phases.

## 5 From block-locality to site-locality

As we highlighted in Section 2, an advantage of the present formalism is that in certain settings it permits a block size of one. That is, the notion of locality in MBQC, which is site-locality, is matched exactly by the notion of locality provided by the formalism. The prior formalism [7, 15, 16] based on matrix product states leads to a larger block size.

We establish block size one for the cluster chain and the cellular automaton states, but find that the same cannot be obtained for the Kitaev Gamma chain.

### 5.1 The cluster chain

We choose blocks  $i = 0, \dots, n + 1$  of size 1. Consistent with the standard discussion of 1D cluster states as resources for MBQC, we take  $n$  to be odd, such that the total chain length is odd as well.

We can choose representations  $u_i, v_{L,i}$  in the bulk and on the left boundary as follows

$$\begin{array}{llll} \text{even sites} & & \text{odd sites} & \\ u_e(g_{01}) = I, & u_e(g_{10}) = X, & u_o(g_{01}) = X, & u_o(g_{10}) = I, \\ v_{L,e}(g_{01}) = Z, & v_{L,e}(g_{10}) = I. & v_{L,o}(g_{01}) = I, & v_{L,o}(g_{10}) = Z. \end{array} \quad (86)$$

The representation  $v_{L,n+1}$  on the right boundary is

$$v_{L,n+1}(g_{01}) = Z, \quad v_{L,n+1}(g_{10}) = X. \quad (87)$$

This concludes the definition of the measurement pattern.

With Eq. (27) we find the representations  $u_{R,i}$  in the bulk and on the left boundary,

$$\begin{aligned} v_{R,e}(g_{01}) &= Z, & v_{R,e}(g_{10}) &= X, \\ v_{R,o}(g_{01}) &= X, & v_{R,o}(g_{10}) &= Z. \end{aligned} \quad (88)$$

With Eq. (24) and Eqs. (86), (88) for  $i = 0$ , we find that  $H = \langle g_{10} \rangle$ . From Eqs. (25) and (26), we compute the sets  $\mathcal{G}_i$ ,  $1 \leq i \leq n$ , finding

$$\begin{aligned} \mathcal{G}_i &= \langle g_{01} \rangle, & \forall i \text{ even}, \\ \mathcal{G}_i &= \langle g_{10} \rangle, & \forall i \text{ odd}. \end{aligned} \quad (89)$$

Inserting Eqs. (86), (62) into Eq. (28) reproduces the global symmetry action Eq. (65),

$$g_{01} \cong ZXIXIXIX\dots IXZ, \quad g_{10} \cong XIXIXIXI\dots IX.$$

The preconditions all hold, and Theorem 1 can be applied.

We now investigate which logical operations follow from the construction. With Eq. (34), the encoded Pauli operators are

$$\overline{T}(g_{01}) = IXI\dots IXZ =: \overline{Z}, \quad \overline{T}(g_{10}) = XIX\dots XIX =: \overline{X},$$

This labeling matches with the corresponding assignments in Eq. (87).

We recall from Eq. (32) that the operators  $R_l(g)$  are defined only for  $g \in \mathcal{G}_l$ , and so are the corresponding string order parameters  $\sigma_l(g) = \langle R_l(g) \rangle_\Phi$ , cf. Eq. (33). With Eq. (89), there exists exactly one string order parameter per site. It is associated with  $g_{01}$  for even and  $g_{10}$  for odd sites. For example, the only non-trivial string order parameter for site  $k = 3$ , with support on sites  $l \geq 3$ , is  $\sigma_3(g_{10}) = \langle IIIZXIX\dots XIX \rangle_\Phi$ .

With Eq. (47), the realizable logical operations  $\overline{V}_k$  hinge on the string order parameters that are defined. Thus, we can perform the following logical CPTP maps by measurement on a single site,

$$\begin{aligned} \overline{V}_k(g_{01}) &= \frac{1+\sigma_k(g_{01})}{2} \left[ e^{-i\frac{\alpha k}{2}\overline{Z}} \right] + \frac{1-\sigma_k(g_{01})}{2} \left[ e^{i\frac{\alpha k}{2}\overline{Z}} \right], & \text{if } k \text{ even}, \\ \overline{V}_k(g_{10}) &= \frac{1+\sigma_k(g_{01})}{2} \left[ e^{-i\frac{\alpha k}{2}\overline{X}} \right] + \frac{1-\sigma_k(g_{01})}{2} \left[ e^{i\frac{\alpha k}{2}\overline{X}} \right], & \text{if } k \text{ odd}. \end{aligned}$$

With Corollary 1, by splitting the realization of a logical operation over many sites, we can arbitrarily closely approximate the unitaries

$$e^{i\alpha Z}, e^{i\beta X}$$

which generate the group  $SU(2)$  as before.

We may now compare to the preceding discussion of the cluster chain in Section 4.5.1. In the present construction, we get one less elementary gate—rotations about the  $y$ -axis. However, from the perspective of computational power, that doesn't make a difference. The group of gates generated is  $SU(2)$  in both cases. Yet, there is a gain in the present construction: the block size has been reduced from 2 to 1. That is, the computational scheme gets by with single-site measurements, which is the standard for MBQC.

## 5.2 The Kitaev-Gamma chain

A site-local scheme is not available here. Any linear representation  $u_i$  that brings the general expression Eq. (28) of the symmetry action on the resource state in agreement with the specific symmetry action Eq. (11) established for the Kitaev Gamma chain requires even block size.

### 5.3 Cellular automaton states

We choose blocks  $i = 1, \dots, n$  of size 1 and both the edge blocks  $i = 0$  and  $n + 1$  of size 2. To be consistent with the framework set up in Section 4.5.3, we choose  $n$  to be divisible by 6. Thus the total number of qubits in the chain is  $6n + 4$ .

We start by choosing representations in the bulk. The site labels below are all mod 6. The projective representations  $v_{L,i}$  are

$$\begin{aligned}
v_{L,1}(g_1) &= I, & v_{L,1}(g_2) &= Z, & v_{L,1}(g_3) &= I, & v_{L,1}(g_4) &= I, \\
v_{L,2}(g_1) &= Z, & v_{L,2}(g_2) &= I, & v_{L,2}(g_3) &= I, & v_{L,2}(g_4) &= I, \\
v_{L,3}(g_1) &= I, & v_{L,3}(g_2) &= I, & v_{L,3}(g_3) &= I, & v_{L,3}(g_4) &= Z, \\
v_{L,4}(g_1) &= I, & v_{L,4}(g_2) &= I, & v_{L,4}(g_3) &= Z, & v_{L,4}(g_4) &= I, \\
v_{L,5}(g_1) &= I, & v_{L,5}(g_2) &= Z, & v_{L,5}(g_3) &= I, & v_{L,5}(g_4) &= I, \\
v_{L,6}(g_1) &= Z, & v_{L,6}(g_2) &= I, & v_{L,6}(g_3) &= I, & v_{L,6}(g_4) &= I,
\end{aligned} \tag{90}$$

and the linear representations  $u_i$  are

$$\begin{aligned}
u_1(g_1) &= X, & u_1(g_2) &= I, & u_1(g_3) &= I, & u_1(g_4) &= I, \\
u_2(g_1) &= I, & u_2(g_2) &= I, & u_2(g_3) &= I, & u_2(g_4) &= X, \\
u_3(g_1) &= I, & u_3(g_2) &= I, & u_3(g_3) &= X, & u_3(g_4) &= I, \\
u_4(g_1) &= I, & u_4(g_2) &= X, & u_4(g_3) &= I, & u_4(g_4) &= X, \\
u_5(g_1) &= X, & u_5(g_2) &= I, & u_5(g_3) &= X, & u_5(g_4) &= I, \\
u_6(g_1) &= I, & u_6(g_2) &= X, & u_6(g_3) &= I, & u_6(g_4) &= I.
\end{aligned} \tag{91}$$

The representations at the left and right boundary are identical to ones mentioned in the Section 4.5.3 via Eqs. 75,76, as their block size remains unchanged. This concludes the specification of the measurement pattern.

Using Eq.27, we find the representations  $v_{R,i}$  in the bulk as

$$\begin{aligned}
v_{R,1}(g_1) &= X, & v_{R,1}(g_2) &= Z, & v_{R,1}(g_3) &= I, & v_{R,1}(g_4) &= I, \\
v_{R,2}(g_1) &= Z, & v_{R,2}(g_2) &= I, & v_{R,2}(g_3) &= I, & v_{R,2}(g_4) &= X, \\
v_{R,3}(g_1) &= I, & v_{R,3}(g_2) &= I, & v_{R,3}(g_3) &= X, & v_{R,3}(g_4) &= Z, \\
v_{R,4}(g_1) &= I, & v_{R,4}(g_2) &= X, & v_{R,4}(g_3) &= Z, & v_{R,4}(g_4) &= X, \\
v_{R,5}(g_1) &= X, & v_{R,5}(g_2) &= Z, & v_{R,5}(g_3) &= X, & v_{R,5}(g_4) &= I, \\
v_{R,6}(g_1) &= Z, & v_{R,6}(g_2) &= X, & v_{R,6}(g_3) &= I, & v_{R,6}(g_4) &= I.
\end{aligned} \tag{92}$$

From Eqs. (25) and (26), we compute the sets  $\mathcal{G}_i$ ,  $1 \leq i \leq n$ , finding

$$\mathcal{G}_i = \begin{cases} \langle g_2 g_4 \rangle, & \forall i = 1 \pmod{6} \\ \langle g_1 g_3 \rangle, & \forall i = 2 \pmod{6} \\ \langle g_4 \rangle, & \forall i = 3 \pmod{6} \\ \langle g_3 \rangle, & \forall i = 4 \pmod{6} \\ \langle g_2 \rangle, & \forall i = 5 \pmod{6} \\ \langle g_1 \rangle, & \forall i = 6 \pmod{6} \end{cases} \tag{93}$$

Inserting Eqs. (77), (91), (76) into Eq. (28) produces

$$\begin{aligned} g_1 &\cong IZ(XIIIIXI) \dots XI, & g_2 &\cong ZX(IIIXIX) \dots ZX, \\ g_3 &\cong XI(IIIXIXI) \dots IZ, & g_4 &\cong ZI(IXIXII) \dots IX. \end{aligned} \quad (94)$$

All constraints are verified, and Theorem 1 can be applied.

Just like the cluster case, in the site local measurement scheme, there exists exactly one string order parameter per site. For example, the only non-trivial string order for site 4 (note that the first two sites are labelled as  $-1$  and  $0$ ), is given by  $\sigma_4(g_3) = \langle IIII ZXI(IIIXIXI) \dots IZ \rangle$ .

Now, coming back to the question of the realizable gate sets with the site local scheme, with Eq. (34), (93) and Corollary 1, we find that we can implement rotations of form

$$e^{i\alpha ZI}, e^{i\beta XZ}, e^{i\gamma IX}, e^{i\delta IZ}, e^{i\tau ZX}, e^{i\eta XI}. \quad (95)$$

Fortunately, these unitaries are enough to generate the whole  $SU(4)$  group.

Comparing the present construction to the block local measurement scheme in Section 4.5.3, we see that we get only 6 elementary gates in the site local case compared to the 15 earlier. But, in the end, it doesn't make any difference as the group of gates generated is  $SU(4)$  in both cases. However, the analysis in this section is better-suited to standard MBQC discussions as we get by with site-local measurements.

## 6 String vs. computational order parameters

Ref. [15] introduced a matrix  $[\nu_{ij}]$  of computational order parameters that can be extracted from the MPS description of the resource state. It governs the effectiveness of MBQC in 1D SPT phases. In the present formalism, precisely the same role is played by the string order parameters  $\sigma_k(g_k)$ ,  $g_k \in \mathcal{G}_k$ . We now demonstrate that these two types of order parameters are related in a simple linear fashion.

We focus on the case of the  $\mathbb{Z}_2 \times \mathbb{Z}_2$ -symmetric cluster phase, which is covered by both the present results and [15]. We use the description in terms of blocks of size 2, cf. Section 4.5.1, which is also used in [15]. Further, we use the additional condition of translation invariance required in [15]. Thus we can eliminate the block label  $k$  in the string order parameters  $\sigma_k(g_k)$ , and henceforth denote them as  $\sigma(g)$ . Finally, we note that Ref. [15] only provides operations in a perturbative expansion in  $\alpha$ , up to linear order, whereas the corresponding expression Eq. (47) contains the full angular dependence. To permit a comparison, in this section we only consider perturbative expansions in  $\alpha$ , up to (including) linear order.

The symmetry-respecting basis is  $\mathcal{B}(0) = \{|0\rangle := |+\rangle|+\rangle, |1\rangle := |-\rangle|+\rangle, |2\rangle := |+\rangle|-\rangle, |3\rangle := |-\rangle|-\rangle\}$ . With this ordering of states, in the notation of [15], the four byproduct operators are<sup>1</sup>

$$C_0 = I, C_1 = -iZ, C_2 = iX, C_3 = -iY.$$

Measuring in the basis of Eq. (18) in [15] results in a rotation, for small rotation angles  $\alpha$ , of  $U(\alpha) = \exp\left(i\alpha \frac{\nu_{10} + \nu_{10}^*}{\nu_{00} + \nu_{11}} Z\right)$ , conditioned upon measuring outcome “0” or “1”. However, Eq. (18) of [15] does not describe the eigenbases of the observables Eq. (31). We need to use instead

$$\mathcal{B}(\alpha) = \left\{ \begin{array}{ll} |0(\alpha)\rangle &= |0\rangle + \frac{\alpha}{2}|1\rangle, & |1(\alpha)\rangle &= |1\rangle - \frac{\alpha}{2}|0\rangle, \\ |2(\alpha)\rangle &= |2\rangle + \frac{\alpha}{2}|3\rangle, & |3(\alpha)\rangle &= |3\rangle - \frac{\alpha}{2}|2\rangle, \end{array} \right\}. \quad (96)$$

<sup>1</sup>The phases of the byproduct operators are subject to convention. Namely, consider the MPS matrices  $A_i = C_i \otimes B_i$ , with  $C_i$  algebraic and constant, and  $B_i$  acting on the ‘junk space’ [7]. The MPS matrices  $A_i$ , and hence the matrix product state described, are invariant under the transformations  $C_i \mapsto e^{i\phi_i} C_i$ ,  $B_i \mapsto e^{-i\phi_i} B_i$ .

Apart from the change in the normalization of the rotation angle  $\alpha$ , the main difference is that not only the states  $|0\rangle$  and  $|1\rangle$  mix, but also the states  $|2\rangle$  and  $|3\rangle$ .

Repeating the calculation of [15] for the measurement basis  $\mathcal{B}(\alpha)$ , we find that the resulting rotation is, to first order in  $\alpha$ ,

$$U(\alpha) = \exp\left(-i\frac{\alpha}{2}(\nu_{10} + \nu_{10}^* + \nu_{23} + \nu_{23}^*)Z\right). \quad (97)$$

We now compare this to the corresponding CPTP map  $\bar{\mathcal{V}}$ . The basis Eq (96) describes the eigenbases of the observables Eq. (31). Specifically, the change of basis from  $\mathcal{B}(0)$  to  $\mathcal{B}(\alpha)$  requires  $v_L(g) = ZI$ , and hence  $g = g_{01}$ . With Eq. (47), to linear order in  $\alpha$ ,

$$\bar{\mathcal{V}}(g_{01}) = \left[\exp\left(-\frac{\alpha}{2}\sigma(g_{01})\bar{Z}\right)\right]. \quad (98)$$

Eqs. (97) and (98) describe the logical operation implemented by the same physical measurement on the same quantum state, hence must agree. This happens only if

$$\sigma(g_{01}) = \nu_{10} + \nu_{10}^* + \nu_{23} + \nu_{23}^*, \quad (99)$$

which is one of the linear relations between  $\sigma(G)$  and  $[\nu]$ . Analogous linear relations can be established between  $\sigma(g_{10})$  and  $\nu_{02}$ ,  $\nu_{13}$ , and between  $\sigma(g_{11})$  and  $\nu_{03}$ ,  $\nu_{12}$ .

## 7 An application: string order and contextuality

Ref. [50] established a connection between string order in symmetry protected topological phases and non-local games [51]—an area at the foundations of quantum physics and information theory. Inspired by this, here we establish a link between string order and quantum contextuality, a subject closely related to non-local games. Our result is stronger in the sense that it applies to an entire symmetry protected phase, not just a sub-region thereof; yet our setting is more permissive.

To begin, we review the notion of quantum contextuality, namely the inviability of non-contextual hidden-variable models [54]. In a non-contextual hidden variable model (nc HVM), pre-determined outcomes  $\lambda_A$  are assigned to observables  $A \in \mathcal{O}$  in such a way that the following conditions are met: (i)  $\lambda_A$  is an eigenvalue of  $A$ ; (ii)  $\lambda_A$  is a function of  $A$  only, and in particular does not depend on what compatible observables  $B, C, \dots$  are measured jointly with  $A$  (context-independence); and (iii) if jointly measurable observables satisfy an algebraic relation,  $X = f(A, B, \dots)$ , the corresponding values satisfy the same relation,  $\lambda_X = f(\lambda_A, \lambda_B, \dots)$ .

If the set  $\mathcal{O}$  is such that the above constraints admit no solutions  $\lambda : \mathcal{O} \rightarrow \mathbb{R}$ , then  $\mathcal{O}$  is called contextual. The Kochen-Specker theorem [52] says that contextual sets  $\mathcal{O}$  exist whenever the Hilbert space dimension is  $\geq 3$ . If a given set  $\mathcal{O}$  does admit solutions  $\lambda : \mathcal{O} \rightarrow \mathbb{R}$ , then one may attempt to mimick the randomness of quantum measurement by a probability distribution  $p$  over the admissible value assignments  $\lambda$ . The notion of state-dependent contextuality then applies:

**Definition 2** *Consider a set  $\mathcal{O}$  of observables for which the set  $\Omega$  of non-contextual value assignments  $\lambda : \mathcal{O} \rightarrow \mathbb{R}$  is non-empty. A state  $|\Psi\rangle$  is contextual wrt.  $\mathcal{O}$  if no probability function  $p : \Omega \rightarrow \mathbb{R}_+$  reproduces the measurement statistics of compatible observables from  $\mathcal{O}$  on  $|\Psi\rangle$ .*

An immediate consequence of this definition is that if  $\mathcal{O} \subset \mathcal{O}'$  and  $|\Psi\rangle$  is contextual wrt.  $\mathcal{O}$  then  $|\Psi\rangle$  is contextual wrt.  $\mathcal{O}'$ . With those notions introduced, we have the following result.



**Theorem 2** Consider a family  $\mathcal{F}_{\Delta,\sigma}$  of short-range entangled states with symmetry group  $\mathbb{Z}_2 \times \mathbb{Z}_2$  acting as in Eq. (7). All states  $|\Psi\rangle \in \mathcal{F}_{\Delta,\sigma}$  have an entanglement range of  $\Delta \leq 0$ , and for all string order parameters it holds that  $|\sigma_k(g)| \geq \sigma > 0$ ,  $g \in \mathcal{G}_k$ , for all sites  $k$ . Further,  $\mathcal{F}_{\Delta,\sigma}$  contains a member of any finite size. Then, the family  $\mathcal{F}_{\Delta,\sigma}$  contains quantum states that are contextual wrt. the set of site-local observables.

*Proof of Theorem 2.* The overall strategy of the proof is to employ MBQC as a *witness* of contextuality, and then invoke Corollary 1 to demonstrate that the witness can be implemented.

(i) *Construction of the contextuality witness.* We derive the witness from the simplest contextual MBQC [53], based on Mermin’s star [54], with two bits of classical input. To accommodate the error that applying Corollary 1 will introduce, we use Theorem 3 of [56], which handles probabilistic MBQCs. For the case of two input bits it says that any MBQC which computes a non-linear Boolean function with a success probability greater than  $3/4$  is contextual.

Concretely, we MBQC-simulate the following set of four quantum circuits, depending on two input bits  $a$  and  $b$ , and yielding one output bit  $s$ ,

$$\frac{I + (-1)^s X}{2} \exp\left(\left(-1\right)^{a+b} i \frac{\pi}{8} Z\right) \exp\left(\left(-1\right)^b i \frac{\pi}{8} Z\right) \exp\left(\left(-1\right)^a i \frac{\pi}{8} Z\right) \exp\left(i \frac{\pi}{8} Z\right) |+\rangle. \quad (100)$$

It is easily verified that this circuit family computes an OR-gate,  $s = a \cup b$ , with unit success probability. The OR-gate is a non-linear Boolean function.

(ii) *Implementation of the contextuality witness.* We choose the one-site blocking discussed in Section 5.1. With Corollary 1 applied to the present case of  $\mathbb{Z}_2 \times \mathbb{Z}_2$  symmetry (the example is completely worked out in Section 5.1) we find that the circuits of Eq. (100) can be realized, with an error that decreases towards zero with increasing size of the resource state, cf. Eq. (51). Since the family  $\mathcal{F}_{\Delta,\sigma}$  contains members of any size, one state is large enough to surpass the contextuality threshold in the success probability of  $3/4$ .  $\square$

Comparing with Theorem 2 in [50], we find that the above Theorem 2 is stronger in the sense that contextuality is established for any non-vanishing value of the string order parameters, not only beyond a threshold value ( $\sigma > 1/3$  in Theorem 2 of [50]). On the other hand, the present contextuality setting is more permissive than the non-local game setting in [50]. Specifically, in the non-local game setting, the sites/blocks on the chain cannot communicate with one another. The contextuality setting above places no such constraint. The measurable observables are local, but which ones among the local observables are measured, and under which conditionings—e.g. on earlier measurement outcomes—is not restricted.

## 8 Conclusion and outlook

We have devised a new framework for MBQC on short-range entangled symmetric resource states. It requires fewer assumptions than previously known. Specifically, we can handle finitely extended systems and understand the effects of boundary, and we do not require translation-invariance. Further, our formalism matches the site-locality of measurements in MBQC, as opposed to interpreting larger blocks of spins as the local unit.

Our physical insight is that, in spatial dimension one, string order gives rise to MBQC computational power. Whenever the string order parameters are non-zero, a constant group of unitary gates can be implemented. The larger the values of the order parameters, the more efficient the implementation. This is the content of Theorem 1 and Corollary 1 in Section 4.3.

Our conceptual insight is that, once we move to finite systems such that SPT phases can no longer form the basis for classification (because they no longer exist), we observe a reversal of importance: the measurement scheme becomes the central object, the object suitable for classification; and the resource state becomes the accessory. The latter has to be symmetric, short-range entangled, and possess string order matching the symmetries; and nothing else about it needs to be known. In the thermodynamic limit discussed in previous works, the essential property of an SPT ordered resource state is the SPT phase it belongs to, characterized by group cohomology. For finite size, this cohomological information reappears in the description of the measurement scheme.

We conclude with the following open questions:

- *Can we classify the MBQC schemes with  $(\mathbb{Z}_2)^m$ -symmetry in spatial dimension one?* We remark that in Section 4.1.2, item 1 of the list of independent constituents of MBQC measurement patterns, we provided the raw material for the classification, i.e. the data to be classified. This data contains projective representations of the symmetry group, as in the classification of SPT phases in 1D. However, because the linear representations—also part of the classification—don’t need to be faithful on individual blocks (see the examples of Section 5), the classification of MBQC schemes in 1D is more complex.
- *Can the present construction be generalized to other symmetry groups?* Likely, the non-Abelian case will differ more from the present treatment than the general Abelian. In this regard, it shall be noted that the first computational phase of quantum matter identified was for a non-Abelian symmetry group,  $S_4$  [14], and that a Wigner-Eckart theorem for MBQC—applicable to both Abelian and non-Abelian symmetry groups—has been established in [55].
- *Can the present computational scheme be generalized to higher spatial dimension?*

**Acknowledgements.** WY, AA and RR are funded from the Canada First Research Excellence Fund, Quantum Materials and Future Technologies Program. AA and RR are funded by USARO (W911NF2010013). WY and AA thank A. Nocera for discussions, and AA and RR thank P. Feldmann, D. Bondarenko, and D.T. Stephen for discussions. The numerical simulations in this work were performed using the software package ITensor [57]. AA thanks E.M. Stoudenmire for software support and discussions.

## A Proof of Corollary 1

*Proof of Corollary 1.* We compare the unitary  $U(\alpha)$  to its approximation by the  $N$ -fold concatenation of the CPTP map  $\mathcal{V}$  with rotation angle  $\propto 1/N$ . We find that the total approximation error is proportional to  $1/N$ ; hence it is of advantage for accuracy to split the rotation into many small parts.

To quantify the error  $\epsilon$  of the total gate operation, we use the diamond norm  $\|\cdot\|_\diamond$  [49], with the properties stated in Lemma 12 therein. In the following we denote the CPTP maps of interest by  $\mathcal{V}_g$ ; it is the group label that matters, not the site label.

For small rotation angles  $\beta$ , that is whenever

$$\frac{\beta}{\sigma(g)} \ll 1,$$

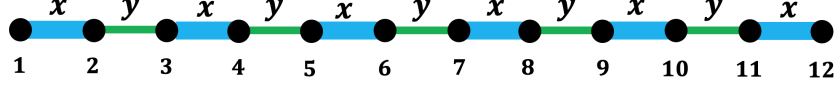


Figure 7: Bond pattern for the 1D bond-alternating Kitaev-Gamma model in the unrotated frame. The thick and thin lines represent the alternating pattern of the bond strengths.

the unitary  $U_g(\beta)$  is best approximated by the CPTP map  $\mathcal{V}_g(\beta/\sigma(g))$ . The approximation error then is

$$\begin{aligned} \|[U_g(\beta)] - \mathcal{V}_g(\beta/\sigma(g))\|_\diamond &\leq \frac{3\beta^2}{4} \frac{1-\sigma(g)^2}{\sigma(g)^2} + O((\beta/\sigma(g))^3) \\ &\leq \beta^2 \frac{1-\sigma^2}{\sigma^2}. \end{aligned} \quad (101)$$

In the last line, we have used the assumption that  $\sigma_k(g) \geq \sigma$ , for all  $k, g \in G$ , and furthermore have bounded the contribution of the trailing orders to  $1/3$  of the leading order contribution to the error. This will always be satisfied for sufficiently small  $\beta$ .

We now bound the error of the  $N$ -fold iteration  $\mathcal{V}\left(\frac{\alpha}{\sigma(g)N}\right)$ . For brevity, we will write  $\mathcal{V}_g[U_g]^{-1}$  for  $\mathcal{V}_g(\alpha/\sigma(g)N)[U_g]^{-1}(\alpha/N)$ . We have that

$$\begin{aligned} \epsilon &= \|[U_g(\alpha)] - \mathcal{V}_g(\alpha/\sigma(g)N)^N\|_\diamond \\ &= \|[U_g(\alpha/N)]^N - \mathcal{V}_g(\alpha/N)^N\|_\diamond \\ &= \|I - (\mathcal{V}_g[U_g]^{-1}(\alpha/N))^N\|_\diamond \\ &= \left\| (I - (\mathcal{V}_g[U_g]^{-1})) \left( I + \mathcal{V}_g[U_g]^{-1} + (\mathcal{V}_g[U_g]^{-1})^2 + \dots + (\mathcal{V}_g[U_g]^{-1})^{N-1} \right) \right\|_\diamond \\ &\leq \|I - (\mathcal{V}_g[U_g]^{-1})\|_\diamond \left\| I + \mathcal{V}_g[U_g]^{-1} + (\mathcal{V}_g[U_g]^{-1})^2 + \dots + (\mathcal{V}_g[U_g]^{-1})^{N-1} \right\|_\diamond \\ &\leq \|I - (\mathcal{V}_g[U_g]^{-1})\|_\diamond \sum_{i=0}^{N-1} \left\| (\mathcal{V}_g[U_g]^{-1})^i \right\|_\diamond \\ &= N \|I - (\mathcal{V}_g[U_g]^{-1})\|_\diamond \\ &= N \|[U_g(\alpha/N)] - \mathcal{V}_g(\alpha/\sigma(g)N)\|_\diamond. \end{aligned}$$

Now combining the above with Eq. (101) for the angle  $\beta = \alpha/N$ , we obtain Eq. (51).  $\square$

## B More on the Kitaev-Gamma chain

### B.1 Hamiltonian in the unrotated frame

The 1D spin-1/2 bond-alternating Kitaev-Gamma model is defined by the following Hamiltonian [35, 36],

$$H_{K\Gamma} = \sum_{\gamma=\langle ij \rangle} g_\gamma [K S_i^\gamma S_j^\gamma + \Gamma(S_i^\alpha S_j^\beta + S_i^\beta S_j^\alpha)], \quad (102)$$

in which  $\gamma \in \{x, y\}$  is the spin direction associated with the bond connecting the nearest neighboring sites  $i$  and  $j$  as shown in Fig. 7, and  $(\gamma, \alpha, \beta)$  form a local right-handed coordinate system in spin space. A useful unitary transformation for studying the 1D Kitaev-Gamma model is the rotation  $U_6$  [33], which acts as  $I, R(\frac{1}{\sqrt{2}}(0, 1, -1), \pi), R(\frac{1}{\sqrt{3}}(1, 1, 1), \frac{2\pi}{3}), R(\frac{1}{\sqrt{2}}(-1, 1, 0), \pi), R(\frac{1}{\sqrt{3}}(1, 1, 1), -\frac{2\pi}{3}), R(\frac{1}{\sqrt{2}}(1, 0, -1), \pi)$  on sites  $1 + 6m, 2 + 6m, 3 + 6m, 4 + 6m, 5 + 6m, 6 + 6m$  ( $m \in \mathbb{Z}$ ), respectively. After the  $U_6$  transformation, the Hamiltonian  $H'_{K\Gamma} = U_6 H_{K\Gamma} (U_6)^{-1}$  acquires the form in Eq. (10) [35, 36]. In this appendix, the spin coordinate systems before and after the  $U_6$  transformation will be termed as unrotated and rotated frames, respectively.

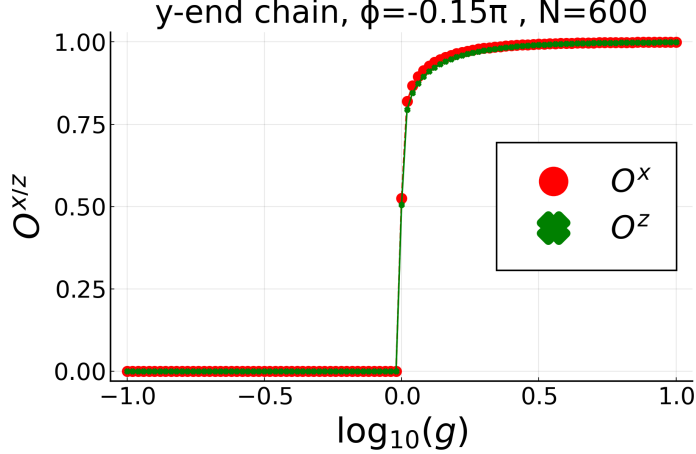


Figure 8: String order parameters  $O^\alpha(\frac{N}{2} + 1, N)$  ( $\alpha = x, z$ ) as functions of  $\log(g)$  at  $\phi = -0.15\pi$  for  $y$ -end chains. DMRG simulations are performed on open chains with system size  $N = 600$ .

There are two duality transformations for the system which are mostly easily seen using  $H_{K\Gamma}$  in Eq. (102) in the unrotated frame [35]:  $U(R(\hat{z}), \pi)$  maps the parameters  $(K, \Gamma, g_x, g_y)$  to  $(K, -\Gamma, g_x, g_y)$ , and  $U(R(\hat{z}), \pi/2)T_a$  maps  $(K, \Gamma, g_x, g_y)$  to  $(K, \Gamma, g_y, g_x)$ . As a result, it is enough to consider the parameter region  $\phi \in (-\pi/2, \pi/2)$ ,  $g \in (0, 1)$ ; and the EH', OH, and OH' phases in Fig. 3 (a) can be obtained from the EH phase by applying  $U(R(\hat{z}, \pi))$ ,  $U(R(\hat{z}, \pi/2))T_a$ , and  $U(R(\hat{z}, -\pi/2))T_a$  in the unrotated frame, respectively, which is the reason why only the EH phase is discussed in Sec. 3.3.2.

## B.2 The odd-Haldane phase

In what follows, an open chain with even length  $N$  will be named as an  $x$ -end (or a  $y$ -end) chain if the bond between the last two sites  $N - 1$  and  $N$  is an  $x$ - (or  $y$ -) bond. As discussed in Sec. 3.3.2, for  $x$ -end chains, the EH phase (and also the EH' phase) has nonvanishing string order parameters  $O_e^\alpha$  ( $\alpha = x, y, z$ ) defined in Eq. (13). On the other hand, since the odd-Haldane phases (i.e., the OH and OH' phases) are related to the even Haldane phases by  $U(R(\pm\hat{z}, \pi/2))T_a$ , it is expected that the string order parameters characterizing the odd-Haldane phases should be defined in  $y$ -end chains with the same expression in Eq. (13).

Fig. 8 shows the numerical values of the string order parameters  $O^\alpha(\frac{N}{2} + 1, N)$  ( $\alpha = x, z$ ) in the rotated frame as a function of  $\log(g)$  for an even-length  $y$ -end chain, where  $\phi$  is fixed to be  $-0.15\pi$ . As is clear in Fig. 8, the string order parameters are nonzero and zero in the  $g > 1$  and  $g < 1$  regions, respectively, which identifies the OH phase in the  $g > 1$  region, in contrast to the EH phase in the  $g < 1$  region. For MBQC purposes,  $y$ -end chains must be used in the OH and OH' phases.

## References

- [1] R. Raussendorf and H.-J. Briegel, *A one-way quantum computer*, Phys. Rev. Lett. **86**, 5188 (2001).

- [2] D. Gross, S. T. Flammia, and J. Eisert, *Most Quantum States Are Too Entangled To Be Useful As Computational Resources*, Phys. Rev. Lett. **102**, 190501 (2009).
- [3] A. C. Doherty and S. D. Bartlett, *Identifying Phases of Quantum Many-Body Systems That Are Universal for Quantum Computation*, Phys. Rev. Lett. **103**, 020506 (2009).
- [4] T. Chung, S. D. Bartlett and A. C. Doherty, *Characterizing measurement-based quantum gates in quantum many-body systems using correlation functions*, Can. J. Phys. **87**, 219 (2009).
- [5] A. Miyake, *Quantum computation on the edge of a symmetry-protected topological order*, Phys. Rev. Lett. **105**, 040501 (2010).
- [6] A.S. Darmawan, G.K. Brennen, S.D. Bartlett, *Measurement-based quantum computation in a two-dimensional phase of matter*, New J. Phys. **14**, 013023 (2012).
- [7] D.V. Else, I. Schwarz, S.D. Bartlett and A.C. Doherty, *Symmetry-protected phases for measurement-based quantum computation*, Phys. Rev. Lett. **108**, 240505 (2012).
- [8] Z.C. Gu and X.G. Wen, *Tensor-entanglement-filtering renormalization approach and symmetry-protected topological order*, Phys. Rev. B **80**, 155131 (2009).
- [9] X. Chen, Z.C. Gu, and X.G. Wen, *Local unitary transformation, long-range quantum entanglement, wave function renormalization, and topological order*, Phys. Rev. B **82**, 155138 (2010).
- [10] Norbert Schuch, David Perez-Garcia, and Ignacio Cirac, *Classifying quantum phases using matrix product states and projected entangled pair states*, Phys. Rev. B **84**, 165139 (2011).
- [11] Yoshiko Ogata, *Classification of symmetry protected topological phases in quantum spin chains*, arXiv:2110.04671.
- [12] X. Chen, Z.C. Gu, Z.X. Liu, X.G. Wen, *Symmetry protected topological orders and the group cohomology of their symmetry group*, Phys. Rev. B **87**, 155114 (2013).
- [13] R. Raussendorf, J. Harrington, K. Goyal, *A fault-tolerant one-way quantum computer*, Ann. Phys. (N.Y.) **321**, 2242 (2006).
- [14] J. Miller and A. Miyake, *Resource Quality of a Symmetry-Protected Topologically Ordered Phase for Quantum Computation*, Phys. Rev. Lett. **114**, 120506 (2015).
- [15] Robert Raussendorf, Dongsheng Wang, Abhishodh Prakash, Tzu-Chieh Wei, David Stephen, *Symmetry-protected topological phases with uniform computational power in one dimension*, Phys. Rev. A **96**, 012302 (2017).
- [16] D.T. Stephen, D.-S. Wang, A. Prakash, T.-C. Wei, R. Raussendorf, Phys. Rev. Lett. **119**, 010504 (2017).
- [17] D.T. Stephen, *Computational power of one-dimensional symmetry-protected topological phases*, MSc Thesis, University of British Columbia (2017).
- [18] R. Raussendorf, C. Okay, D.-S. Wang, D. T. Stephen, and H. P. Nautrup, *Computationally universal phase of quantum matter*, Phys. Rev. Lett. **122**, 090501 (2019).
- [19] T. Devakul and D.J. Williamson, *Universal quantum computation using fractal symmetry-protected cluster phases*, Phys. Rev. A **98**, 022332 (2018).

- [20] David T. Stephen, Hendrik Poulsen Nautrup, Juani Bermejo-Vega, Jens Eisert, Robert Raussendorf, *Subsystem symmetries, quantum cellular automata, and computational phases of quantum matter*, Quantum **3**, 142 (2019).
- [21] Austin K. Daniel, Rafael N. Alexander, Akimasa Miyake, *Computational universality of symmetry-protected topologically ordered cluster phases on 2D Archimedean lattices*, Quantum **4**, 228 (2020).
- [22] A. Miyake, *Quantum computational capability of a 2D valence bond solid phase*, Ann. Phys. **326**, 1656-1671 (2011).
- [23] Tzu-Chieh Wei, Ian Affleck, Robert Raussendorf, *The Affleck-Kennedy-Lieb-Tasaki State on a Honeycomb Lattice is a Universal Quantum Computational Resource*, Phys. Rev. Lett. **106**, 070501 (2011).
- [24] Sam Roberts and Stephen D. Bartlett, *Symmetry-Protected Self-Correcting Quantum Memories*, Phys. Rev. X **10**, 031041 (2020).
- [25] Gabriel Wong, Robert Raussendorf, Bartłomiej Czech *The Gauge Theory of Measurement-Based Quantum Computation*, arXiv:2207.10098.
- [26] M. den Nijs and K. Rommelse, *Preroughening transitions in crystal surfaces and valence-bond phases in quantum spin chains*, Phys. Rev. B **40**, 4709 (1989).
- [27] H. Tasaki, *Quantum liquid in antiferromagnetic chains: A stochastic geometric approach to the Haldane gap*, Phys. Rev. Lett. **66**, 798 (1991).
- [28] D. Perez-Garcia, M.M. Wolf, M. Sanz, F. Verstraete, and J.I. Cirac, *String Order and Symmetries in Quantum Spin Lattices*, Phys. Rev. Lett. **100**, 167202 (2008).
- [29] A. Molnar, J. Garre-Rubio, D. Perez-Garcia, N. Schuch, J.I. Cirac, *Normal projected entangled pair states generating the same state*, New J. Phys. **20**, 113017 (2018).
- [30] J.I. Cirac, D. Perez-Garcia, N. Schuch, and F. Verstraete, *Matrix product states and projected entangled pair states: Concepts, symmetries, theorems*, Rev. Mod. Phys. **93**, 045003 (2021).
- [31] M.B. Hastings, *Lieb-Schultz-Mattis in higher dimensions*, Phys. Rev. B **69**, 104431 (2004).
- [32] C. E. Agrapidis, J. van den Brink, and S. Nishimoto, *Ordered states in the Kitaev-Heisenberg model: From 1D chains to 2D honeycomb*, Sci. Rep. **8**, 1815 (2018).
- [33] W. Yang, A. Nocera, T. Tummuru, H.-Y. Kee, and I. Affleck, *Phase Diagram of the Spin-1/2 Kitaev-Gamma Chain and Emergent  $SU(2)$  Symmetry*, Phys. Rev. Lett. **124**, 147205 (2020).
- [34] W. Yang, A. Nocera, and I. Affleck, *Comprehensive study of the phase diagram of the spin-1/2 Kitaev-Heisenberg-Gamma chain*, Phys. Rev. Research **2**, 033268 (2020).
- [35] Q. Luo, J. Zhao, X. Wang, and H.-Y. Kee, *Unveiling the phase diagram of a bond-alternating spin- $\frac{1}{2}$   $K$ - $\Gamma$  chain*, Phys. Rev. B **103**, 144423 (2021).
- [36] W. Yang, A. Nocera, P. Herringer, R. Raussendorf, I. Affleck, *Symmetry analysis of bond-alternating Kitaev spin chains and ladders*, Phys. Rev. B **105**, 094432 (2022).

- [37] W. Yang, A. Nocera, C. Xu, H.-Y. Kee, I. Affleck, *Counter-rotating spiral, zigzag, and  $120^\circ$  orders from coupled-chain analysis of Kitaev-Gamma-Heisenberg model, and relations to honeycomb iridates*, arXiv:2207.02188 (2022).
- [38] A. Kitaev, *Anyons in an exactly solved model and beyond*, Ann. Phys. (N. Y). **321**, 2 (2006).
- [39] C. Nayak, S. H. Simon, A. Stern, M. Freedman, and S. Das Sarma, *Non-Abelian anyons and topological quantum computation*, Rev. Mod. Phys. **80**, 1083 (2008).
- [40] G. Jackeli and G. Khaliullin, *Mott Insulators in the Strong Spin-Orbit Coupling Limit: From Heisenberg to a Quantum Compass and Kitaev Models*, Phys. Rev. Lett. **102**, 017205 (2009).
- [41] J. G. Rau, E. K. H. Lee, and H. Y. Kee, *Generic spin model for the honeycomb iridates beyond the Kitaev limit*, Phys. Rev. Lett. **112**, 077204 (2014).
- [42] J. G. Rau, E. K.-H. Lee, and H.-Y. Kee, *Spin-Orbit Physics Giving Rise to Novel Phases in Correlated Systems: Iridates and Related Materials*, Annu. Rev. Condens. Matter Phys. **7**, 195 (2016).
- [43] S. M. Winter, A. A. Tsirlin, M. Daghofer, J. van den Brink, Y. Singh, P. Gegenwart, and R. Valentí, *Models and materials for generalized Kitaev magnetism*, J. Phys. Condens. Matter **29**, 493002 (2017).
- [44] M. Hermanns, I. Kimchi, and J. Knolle, *Physics of the Kitaev Model: Fractionalization, Dynamic Correlations, and Material Connections*, Annu. Rev. Condens. Matter Phys. **9**, 17 (2018).
- [45] F. D. M. Haldane, *Nonlinear field theory of large-spin Heisenberg antiferromagnets: semiclassically quantized solitons of the one-dimensional easy-axis Néel state*, Phys. Rev. Lett. **50**, 1153 (1983).
- [46] I. Affleck, T. Kennedy, E. H. Lieb, and H. Tasaki, *Rigorous results on valence-bond ground states in antiferromagnets*, Phys. Rev. Lett. **59**, 799 (1987).
- [47] X. Chen, Z.-C. Gu, and X.-G. Wen, *Classification of gapped symmetric phases in one-dimensional spin systems*, Phys. Rev. B **83**, 035107 (2011).
- [48] David T. Stephen, Wen Wei Ho, Tzu-Chieh Wei, Robert Raussendorf, Ruben Verresen, *Universal measurement-based quantum computation in a one-dimensional architecture enabled by dual-unitary circuits*, arXiv:2209.06191.
- [49] D. Aharonov, A. Kitaev, N. Nisan, *Quantum circuits with mixed states*, Proc. of the 30th Annual ACM Symposium on Theory of Computing, and quant-ph/9806029 (1998).
- [50] Austin K. Daniel and Akimasa Miyake, *Quantum Computational Advantage with String Order Parameters of One-Dimensional Symmetry-Protected Topological Order*, Phys. Rev. Lett. **126**, 090505 (2021).
- [51] G. Brassard, A. Broadbent, and A. Tapp, *Quantum Pseudo-Telepathy*, Foundations of Physics **35**, 1877 (2005).
- [52] S. Kochen and E. P. Specker, *The Problem of Hidden Variables in Quantum Mechanics*, J. Math. Mech. **17**, 59 (1967).

- [53] Janet Anders, Dan E. Browne, *Computational power of correlations*, Phys. Rev. Lett. 102, 050502 (2009).
- [54] N. David Mermin, *Hidden variables and the two theorems of John Bell*, Rev. Mod. Phys. 65, 803 (1993).
- [55] Abhishodh Prakash, Tzu-Chieh Wei, *Ground states of 1D symmetry-protected topological phases and their utility as resource states for quantum computation*, Phys. Rev. A 92, 022310 (2015).
- [56] Robert Raussendorf, *Contextuality in measurement-based quantum computation*, Phys. Rev. A **88**, 022322 (2013).
- [57] Matthew Fishman, Steven R. White, E. Miles Stoudenmire, *The ITensor Software Library for Tensor Network Calculations*, SciPost Phys. Codebases 4 (2022).